Cancer Cell

Article

Fungal mycobiome drives IL-33 secretion and type 2 immunity in pancreatic cancer

Graphical abstract

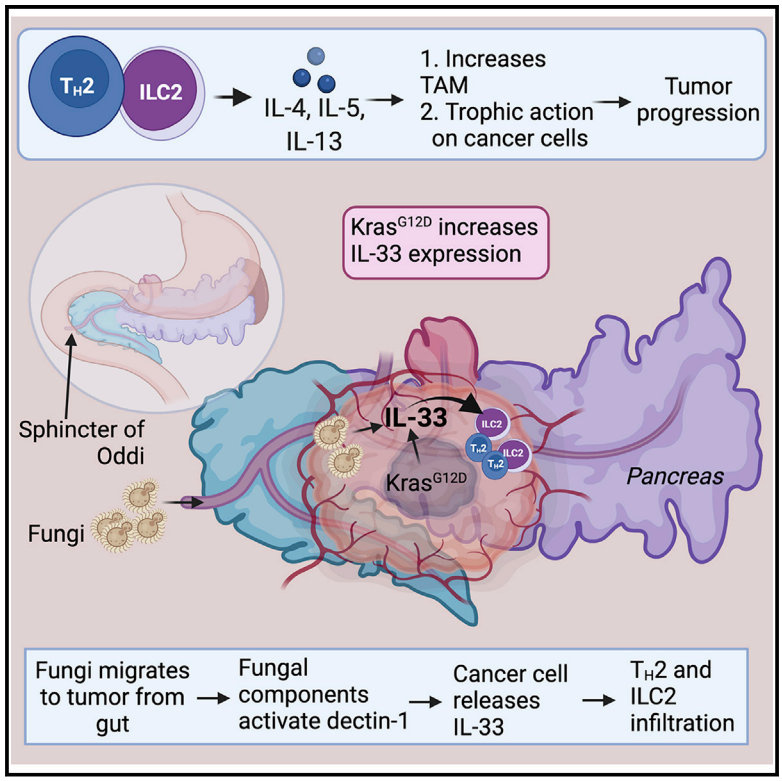

Highlights

- Oncogenic KRAS^{G12D} upregulates IL-33 to promote type 2 immunity in PDAC
- Intratumoral mycobiome enhances cancer cell secretion of IL-33
- Secreted IL-33 recruits and activates T_H2 and ILC2 cells in the PDAC TME
- Genetic deletion of IL-33 or anti-fungal treatment causes PDAC tumor regression

Authors

Aftab Alam, Eric Levanduski, Parker Denz, ..., Scott I. Abrams, Brahm H. Segal, Prasenjit Dey

Correspondence

prasenjit.dey@roswellpark.org

In brief

Alam et al. discover that IL-33 is a downstream target of Kras^{G12D}. Furthermore, he reports that intratumor mycobiome activates a signaling pathway in cancer cells that facilitate IL-33 secretion. The secretion of IL-33 promotes type 2 immune response and accelerates pancreatic cancer progression.

Alam et al., 2022, Cancer Cell *40*, 1–15
February 14, 2022
https://doi.org/10.1016/j.ccell.2022.01.003

CellPress

Please cite this article in press as: Alam et al., Fungal mycobiome drives IL-33 secretion and type 2 immunity in pancreatic cancer, Cancer Cell (2022), https://doi.org/10.1016/j.ccell.2022.01.003

Cancer Cell

CellPress

Article

Fungal mycobiome drives IL-33 secretion and type 2 immunity in pancreatic cancer

Aftab Alam,[1] Eric Levanduski,[1] Parker Denz,[1] Helena Solleiro Villavicencio,[1,13] Maulasri Bhatta,[1] Lamees Alhorebi,[1] Yali Zhang,[2] Eduardo Cortes Gomez,[2] Brian Morreale,[1] Sharon Senchanthisai,[1] Jun Li,[3] Steven G. Turowski,[4] Sandra Sexton,[5] Sheila Jani Sait,[6] Prashant K. Singh,[7] Jianmin Wang,[2] Anirban Maitra,[8] Pawel Kalinski,[1,9] Ronald A. DePinho,[10] Huamin Wang,[11] Wenting Liao,[12] Scott I. Abrams,[1] Brahm H. Segal,[9] and Prasenjit Dey[1,14,*]

[1]Department of Immunology, Roswell Park Comprehensive Cancer Center, Elm & Carlton Sts. CGP/BLSC-L5307, Buffalo, NY 14263, USA
[2]Department of Biostatistics and Bioinformatics, Roswell Park Comprehensive Cancer Center, Buffalo, NY 14263, USA
[3]Department of Genomic Medicine, The University of Texas MD Anderson Cancer Center, Houston, TX 77030, USA
[4]Department of Cell Stress Biology, Roswell Park Comprehensive Cancer Center, Buffalo, NY 14263, USA
[5]Department of Animal Resources, Roswell Park Comprehensive Cancer Center, Buffalo, NY 14263, USA
[6]Department of Cytogenetics, Roswell Park Comprehensive Cancer Center, Buffalo, NY 14263, USA
[7]Genomics Shared Resource, Department of Cancer Genetics & Genomics, Roswell Park Comprehensive Cancer Center, Buffalo, NY 14263, USA
[8]Department of Translational Molecular Pathology, The University of Texas MD Anderson Cancer Center, Houston, TX 77030, USA
[9]Department of Medicine, Roswell Park Comprehensive Cancer Center, Buffalo, NY 14263, USA
[10]Department of Cancer Biology, The University of Texas MD Anderson Cancer Center, Houston, TX 77030, USA
[11]Department of Pathology, The University of Texas MD Anderson Cancer Center, Houston, TX 77030, USA
[12]Collaborative Innovation Center for Cancer Medicine, State Key Laboratory of Oncology in South China, Sun Yat-sen University Cancer Center, Guangzhou 510060, China
[13]Present address: Posgrado en Ciencias Genómicas, Universidad Autónoma de la Ciudad de, Mexico City, CP 06720, Mexico
[14]Lead contact
*Correspondence: prasenjit.dey@roswellpark.org
https://doi.org/10.1016/j.ccell.2022.01.003

SUMMARY

T_H2 cells and innate lymphoid cells 2 (ILC2) can stimulate tumor growth by secreting pro-tumorigenic cytokines such as interleukin-4 (IL-4), IL-5, and IL-13. However, the mechanisms by which type 2 immune cells traffic to the tumor microenvironment are unknown. Here, we show that oncogenic *Kras*^{G12D} increases IL-33 expression in pancreatic ductal adenocarcinoma (PDAC) cells, which recruits and activates T_H2 and ILC2 cells. Correspondingly, cancer-cell-specific deletion of IL-33 reduces T_H2 and ILC2 recruitment and promotes tumor regression. Unexpectedly, IL-33 secretion is dependent on the intratumoral fungal mycobiome. Genetic deletion of IL-33 or anti-fungal treatment decreases T_H2 and ILC2 infiltration and increases survival. Consistently, high IL-33 expression is observed in approximately 20% of human PDAC, and expression is mainly restricted to cancer cells. These data expand our knowledge of the mechanisms driving PDAC tumor progression and identify therapeutically targetable pathways involving intratumoral mycobiome-driven secretion of IL-33.

INTRODUCTION

Pancreatic ductal adenocarcinoma (PDAC) is associated with a distinctive tumor immune profile dominated by immune-suppressor cells, such as tumor-associated macrophages (TAMs), T regulatory (T_{reg}) cells, $CD4^+$ T_H2 cells, and myeloid-derived suppressor cells (MDSCs), which act in concert to inhibit effector T cell activation, expansion, and function, thereby contributing to suppression of anti-tumor T cell immunity and PDAC progression (Clark et al., 2007; Steele et al., 2013; Feig et al., 2012). In addition to its classical roles in tumor immunity, immune cells can contribute to additional cancer hallmarks including a unique metabolic mechanism by which $CD4^+$ T_H2 cells support glycolysis to fuel PDAC progression (Dey et al., 2020). Specifically, T_H2 cells infiltrate the pancreas in the early stages of tumorigenesis and secrete type 2 cytokines (interleukin-4 [IL-4] and IL-13) that promote metabolic reprogramming and proliferation of cancer cells in murine *Kras*^{G12D}-driven PDAC. Consistent with type 2 immune responses driving PDAC progression in mouse models, PDAC patients with predominantly T_H2 ($CD45^+CD3^+CD4^+Gata3^+$)-polarized lymphoid cell infiltration exhibit reduced survival compared with patients with a higher infiltration of T_H1 ($CD45^+CD3^+CD4^+Tbet^+$) cells (De Monte et al., 2011). Moreover, the circulating levels of IL-4 negatively correlate with disease-free survival in PDAC patients (Piro et al., 2017).

Please cite this article in press as: Alam et al., Fungal mycobiome drives IL-33 secretion and type 2 immunity in pancreatic cancer, Cancer Cell (2022), https://doi.org/10.1016/j.ccell.2022.01.003

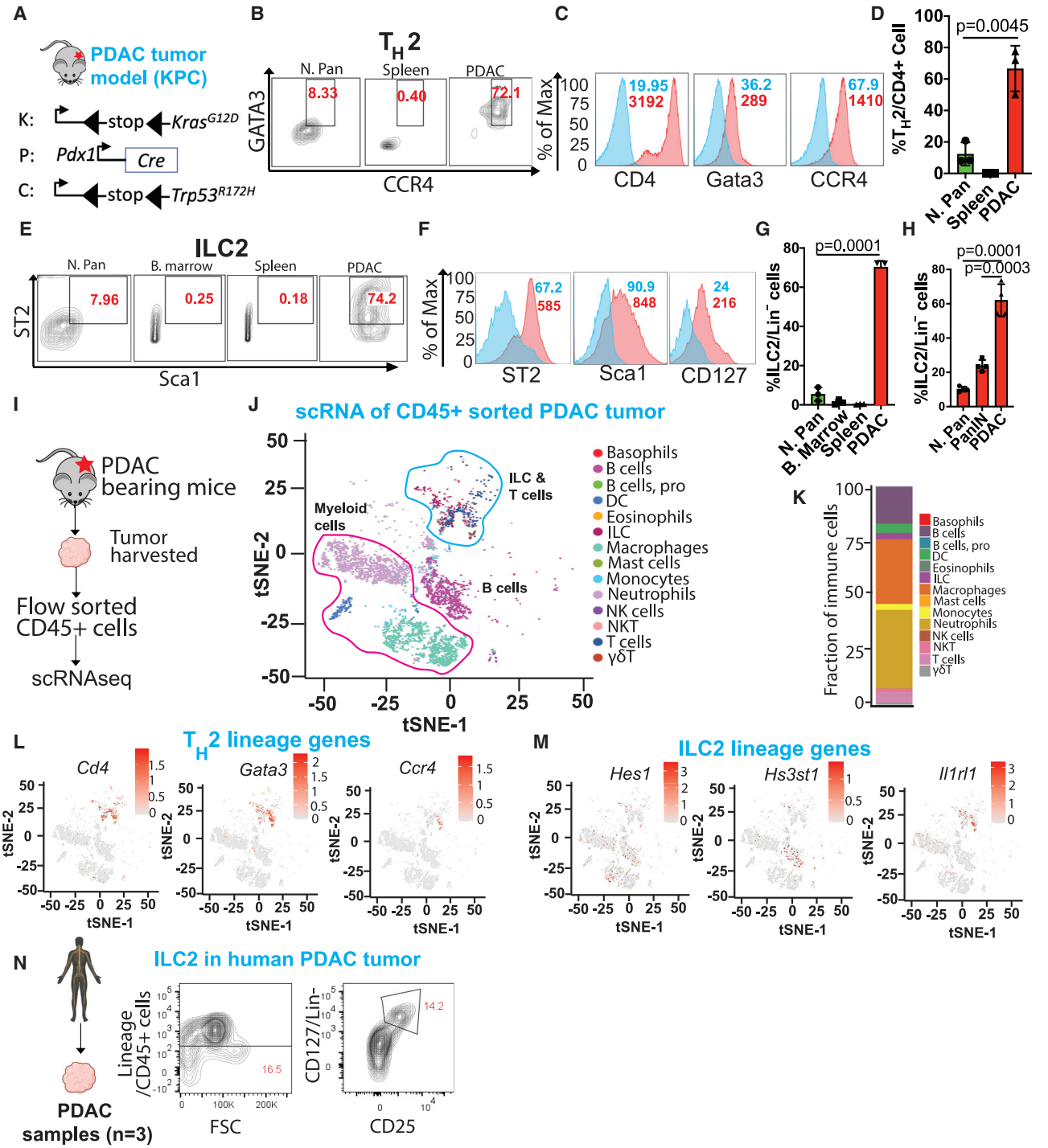

Figure 1. Type 2 immune cell infiltration increases significantly in PDAC tumor microenvironment

(A) Schematic showing the strategy for KPC (*Kras^{G12D}; Trp53^{R172H}; pdx-Cre*) PDAC mouse modeling.

(B) Flow cytometry gating strategy and frequency of T_H2 cells out of total $CD4^+$ T cells in normal pancreas, spleen, and PDAC tumor.

(C) Representative flow cytometry histogram of T_H2 cell phenotype stained with isotype control (blue histogram) and CD4, Gata3, and CCR4 antibodies (red histogram).

(D) Frequency of T_H2 cells out of total $CD4^+$ T cells in normal pancreas, spleen, and PDAC tumor (n = 3).

(E) Gating strategy and frequency of ILC2 cells out of total lineage-negative (Lin^-) (CD3, Ly6G, Ly6C, CD11b, CD45R/B220, and TER-119) cells in normal pancreas, bone marrow, spleen, and PDAC tumor (n = 3).

(F) Representative flow cytometry histogram of ILC2 cell phenotype stained with isotype control (blue histogram) and ST2, Sca-1, and CD127 antibodies (red histogram).

(legend continued on next page)

Please cite this article in press as: Alam et al., Fungal mycobiome drives IL-33 secretion and type 2 immunity in pancreatic cancer, Cancer Cell (2022), https://doi.org/10.1016/j.ccell.2022.01.003

Given the emerging importance of T_H2 cells in PDAC (Dey et al., 2020), we sought to determine the molecular mechanisms driving their recruitment and expansion in the tumor microenvironment (TME). Our studies identified oncogenic $KRAS^{G12D}$-mediated upregulation of IL-33, which is a known potent activator of T_H2, innate lymphoid cells 2 (ILC2), T_{regs}, and eosinophils (Liew et al., 2016). IL-33 is both a damage-associated molecular pattern (DAMP) and a cytokine that belongs to the IL-1 cytokine superfamily (Schmitz et al., 2005), which plays important roles in innate immunity, inflammation, and tumor development (Wang et al., 2017; Fournie and Poupot, 2018; Li et al., 2019; Cui et al., 2018). IL-33 exerts its biological function by binding to its cognate receptor, suppression of tumorigenicity 2 (ST2; also called IL1RL1) (Lingel et al., 2009), which interacts with its co-receptor, the IL-1 receptor accessory protein (IL1RAcP) (Lingel et al., 2009). Both receptors are expressed by innate and type 2 immune cells that include T_H2 cells, ILC2s, T_{regs}, eosinophils, basophils, and mast cells (Rank et al., 2009; Ali et al., 2007).

ILC2s are the most prominent target of IL-33 and stimulate the activation of ILC2 in response to several stimuli, such as allergens and parasites. ILC2s are primarily tissue-resident immunocytes that remain in close proximity to the epithelial cells, enabling ILC2 cells to respond to an immune insult within hours by producing cytokines such as IL-4, IL-13, and IL-5, which in turn activate additional players of the type 2 immune response (Van Gool et al., 2014; Vivier et al., 2018). Moreover, activation of ILC2 cells is independent of antigen presentation and uses ligand receptors often specific to the tissue where they reside.

Gut microbes can interact with the host and modulate disease pathogenesis and response to therapy (Gopalakrishnan et al., 2018; Matson et al., 2018). It is now well known that microbes can colonize the pancreas and play a role in PDAC tumorigenesis and progression (Riquelme et al., 2019; Aykut et al., 2019). Specifically, a recent study found that the mycobiome present in the gut lumen migrates to the pancreas via the sphincter of Oddi (Aykut et al., 2019). The translocation of endoluminal fungi to the pancreas allows the fungal population to increase by >3,000-fold in PDAC compared with the normal pancreas.

In this study, oncogenic $Kras^{G12D}$ is shown to induce IL-33 expression and secretion by cancer cells through a pathway that depends on fungi within the TME and that genetic deletion of IL-33 or anti-fungal treatment each lead to robust PDAC tumor regression. This mechanism of cooperative interactions of intratumor fungi with cancer cells and priming type 2 immune responses to accelerate tumor progression identifies potential therapeutic strategies for PDAC.

RESULTS

Type 2 immune cell infiltration increases significantly in PDAC tumor microenvironment

The observations that $CD4^+Gata3^+$ T_H2 cells infiltrate the TME and promote tumorigenesis via IL-4 and IL-13 (Venmar et al., 2015; Dey et al., 2020) prompted a more thorough characterization of the type 2 immunocytes present within the PDAC tumors of KPC ($Kras^{G12D}$; $Trp53^{R172H}$; *Pdx-Cre*) mice (Figure 1A). Flow cytometry (Figure S1A) revealed a dramatic expansion of T_H2 ($CD4^+Gata3^+CCR4^+$) cells within the $CD4^+$ T cell population in the PDAC TME (72.1%) compared with the normal pancreas (8.33%) and spleen (0.4%) (Figures 1B–1D and S1B). This was accompanied by a significant increase in ILC2 cells ($Lin^-Sca1^+ST2^+$) in the PDAC TME (74.2%) compared with the normal pancreas (7.96%), spleen (0.18%), and bone marrow (0.25%) (Figures 1E–1G and S1C). Specifically, the frequency of ILC2 cells was approximately 60% of lineage-negative (Lin^-) cells in the PDAC (KPC model) compared with <10% in the normal pancreas and ~25% in PanIN (Figure 1H). Similarly, the frequency of ILC2 cells was approximately 45% of Lin^- cells in the PDAC (iKPC model) compared with <10% in the normal pancreas (Figure S1D).

To solidify our flow-based immunophenotyping data, we used single-cell RNA sequencing (scRNA-seq) analysis to identify the presence of the type 2 immunocytes in the PDAC TME. We sort-purified $CD45^+$ cells and used the 10X Genomics platform for scRNA-seq of the immune populations in the PDAC tumor samples (Figures 1I and 1J). The majority of immune cell populations identified were myeloid cells (macrophages, monocytes, dendritic cells [DCs], and neutrophils: ~74.72%), followed by lymphoid populations (16.45%) (Figures 1K and S1E). Using previously reported gene signatures for T_H2 (Tibbitt et al., 2019) and ILC2 (Robinette et al., 2015), we found that the T_H2 cluster was enriched for *Cd4*, *Gata3*, and *Ccr4* genes (Figures 1L and S1F) and ILC2 clusters were enriched for *Hes1*, *Hs3st1*, and *Il1rl1* genes (Figures 1M and S1G), which are bona fide markers of T_H2 and ILC2 cells, respectively. Finally, we analyzed fresh human PDAC samples by flow cytometry and found that ILC2 cells accounted for 14.2% of the Lin^- cells (Figure 1N). Overall, these results show that the murine and human PDAC TME contain abundant T_H2 and ILC2s cells.

IL-33 is a downstream target of oncogenic $Kras^{G12D}$

Type 2 immunocytes are detected in the early stages of PDAC tumorigenesis (Dey et al., 2020), prompting speculation that a chemotactic factor secreted by cancer cells may recruit and

(G) Frequency of ILC2 cells out of total Lin^- cells in normal pancreas, bone marrow, spleen, and PDAC tumor (n = 4).
(H) Frequency of ILC2 cells out of total Lin^- cells in normal pancreas, PanIN, and PDAC tumor (n = 4).
(I) Schematic showing the experimental strategy for single-cell RNA sequencing (scRNA-seq) from PDAC tumor-bearing mice. $CD45^+$ cells were flow-sorted from PDAC tumor and 10,000 live $CD45^+$ cells were used for scRNA-seq.
(J) t-SNE plot of immune cells showing 14 clusters belonging to three major groups in PDAC sample.
(K) Bar graph showing the proportion of major immune cell clusters in PDAC sample.
(L) t-SNE plots showing T_H2 lineage genes (*Cd4*, *Gata3*, and *Ccr4*) expression in subcluster of immune cells. The color key bar represents gene expression level.
(M) t-SNE plots showing expression of ILC2 lineage genes (*Hes1*, *Hs3st1*, and *Il1rl1*) expression in subcluster of immune cells. The color key represents gene expression level.
(N) Gating and frequency of ILC2 out of total Lin^- (CD3, CD14, CD16, CD19, CD20, and CD56) cells in human PDAC tumor.
Data are presented as mean ± SD. p values were calculated using Student's t test. ns, no significance. Individual p values are indicated in the panels. See also Figure S1.

Please cite this article in press as: Alam et al., Fungal mycobiome drives IL-33 secretion and type 2 immunity in pancreatic cancer, Cancer Cell (2022), https://doi.org/10.1016/j.ccell.2022.01.003

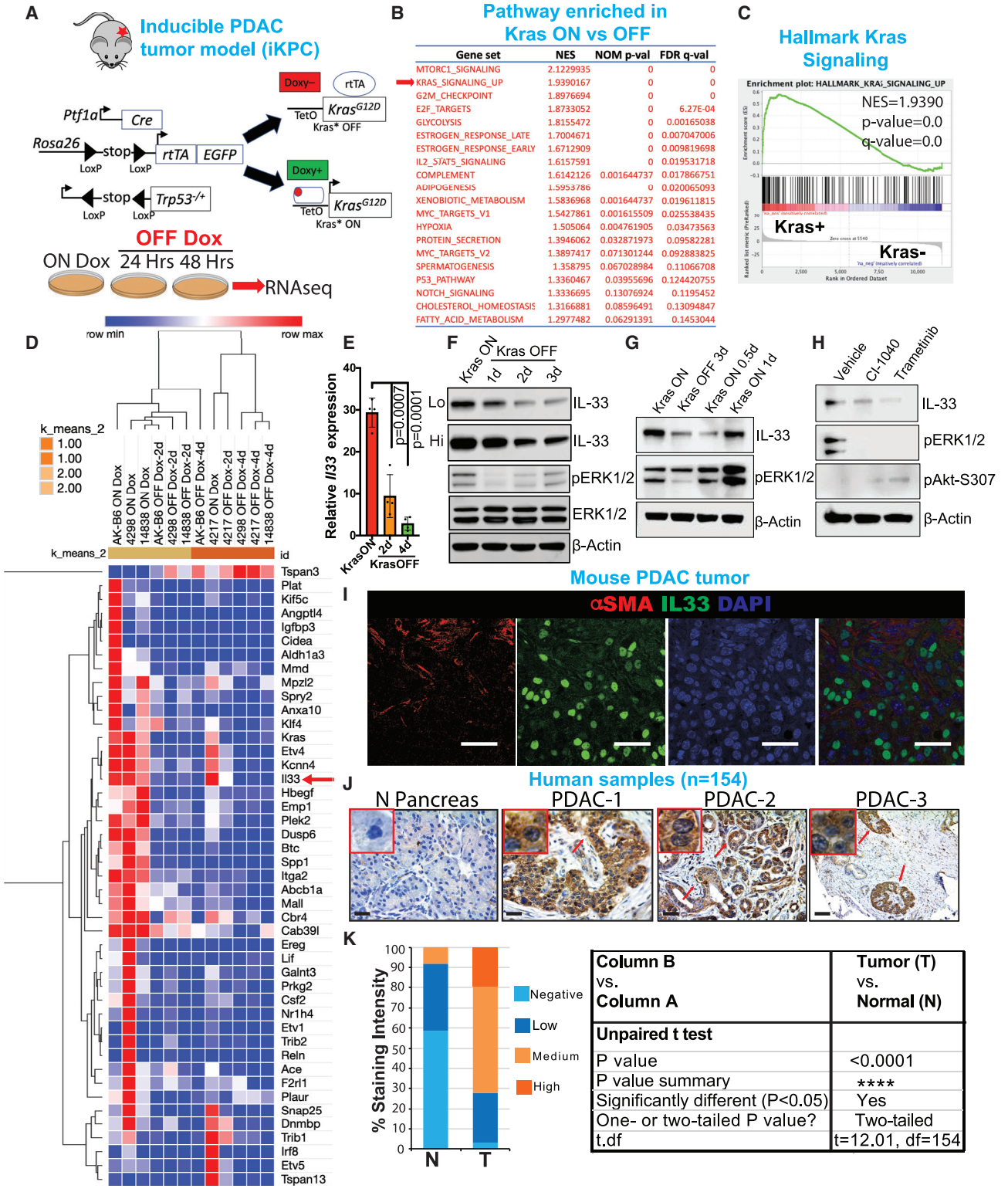

Column B vs. Column A	Tumor (T) vs. Normal (N)
Unpaired t test	
P value	<0.0001
P value summary	****
Significantly different (P<0.05)	Yes
One- or two-tailed P value?	Two-tailed
t.df	t=12.01, df=154

Figure 2. IL-33 is a downstream target of oncogenic *Kras*^{G12D}

(A) Schematic showing doxycycline (Dox)-inducible *Kras*^{G12D} transgenic mouse model (iKPC) (top). Strategy to turn Kras signaling ON and OFF in cell lines followed by transcriptome analysis (bottom).

(B) Pathways enriched upon gene set enrichment analysis of RNA-seq dataset comparing Kras ON and Kras OFF.

(C) GSEA analysis of RNA-seq dataset showing enrichment of hallmark Kras signaling comparing Kras ON and Kras OFF.

(legend continued on next page)

Please cite this article in press as: Alam et al., Fungal mycobiome drives IL-33 secretion and type 2 immunity in pancreatic cancer, Cancer Cell (2022), https://doi.org/10.1016/j.ccell.2022.01.003

activate them. Given that KRAS mutation is an early genetic alteration and drives tumor initiation, we examined the *Kras*^{G12D}-regulated transcript of multiple PDAC cell lines derived from the inducible model of PDAC (iKPC: LSL-tet-*O*-*Kras*^{G12D}; LSL-*Trp53*$^{+/-}$; *p48-Cre*;LSL-*Rosa26-rtTA*) (Figure 2A) (Ying et al., 2016). RNA-seq analysis of iKPC cell lines included *Kras*^{G12D} ON (doxycycline ON), *Kras*^{G12D} OFF 2 days, and *Kras*^{G12D} OFF 4 days. Among the top cytokine genes that are regulated by *Kras*^{G12D} and enriched in the KRAS signaling network is the alarmin gene, *Il33* (Figures 2B–2D). *Il33* expression is ~30-fold higher in *Kras*^{G12D} ON compared with *Kras*^{G12D} OFF (4 days) samples, as validated by quantitative real-time PCR (qRT-PCR) analysis (Figures 2E, S2A, and S2B).

The above findings were further validated by western blot analysis showing a loss of IL-33 expression upon abolishing *Kras*^{G12D} signaling (Figures 2F and 2G). We further validated this finding using cell lines derived from the KPC model. Treatment with MEK inhibitors (CI-1040 and trametinib), a downstream target of KRAS signaling, resulted in complete inhibition of IL-33 expression in these cell lines (Figures 2H and S2C). However, treatment with PI3K inhibitors (buparlisib and GSK-690696) did not lead to a reduction in IL-33 expression, suggesting that IL-33 is induced via a KRAS-MEK-ERK signaling pathway independent of PI3K (Figure S2C).

We next evaluated IL-33 expression in the KPC mouse model and human PDAC tissue. In the KPC model, IL-33 expression was mostly observed in the cancer cells with nominal expression observed in the stromal compartment (Figure 2I). Furthermore, these murine data align with the human tumor data showing that IL-33 expression was increased, with ~20% PDAC cases showing high and ~52% showing moderate IL-33 expression (Figures 2J and 2K). As with mice, IL-33 expression in human PDAC specimens was most prominent in cancer cells with minimal staining in the stromal compartment (Figures 2J, S2D, and S2E). The normal pancreas did not express detectable IL-33 (Figures 2J and S2F). These data show that *Kras*^{G12D}-MEK signaling induces IL-33 in PDAC cells.

IL-33 expression is required for the recruitment and activation of type 2 immunocytes

T_H2 and ILC2 cellular infiltration increases significantly during PDAC tumorigenesis. To test the requirement of IL-33 expression by cancer cells to recruit type 2 immunocytes, we depleted *Il33* in cancer cells by lentivirus transduction of small hairpin RNA (shRNA) (Figures 3A and 3B). While shRNA-mediated depletion of *Il33* had no effect on cell growth *in vitro* (Figure S3A), decreased *Il33* levels in cancer cells resulted in reduced tumor burden and increased survival in a syngeneic orthotopic model of PDAC (Figures 3C, 3D, S3B, and S3C). Immunofluorescence of these tumors confirmed that PDAC cancer cells are the major source of IL-33 and that the IL-33 signal is diminished by shRNA-mediated depletion (Figure 3E). Moreover, malignant ascites, observed in ~20% of PDAC patients (Zervos et al., 2006), is also a feature of the PDAC mouse model. In tumor-bearing mice, *Il33* depletion in cancer cells led to decreased IL-33 protein levels in the ascites fluid (Figure 3F).

In establishing the mechanistic link between IL-33 secretion and ILC2 trafficking, flow cytometry analysis of the TME showed that *Il33* depletion reduced both T_H2 and ILC2 infiltration (Figures 3G, 3H, and S3D–S3G). In addition to ILC2 and T_H2 cells, T_{reg} cells are known to express ST2 and respond to IL-33 signaling (Pastille et al., 2019). Accordingly, IL-33 depletion resulted in a small but significant reduction in T_{reg} infiltration in the TME (Figure 3I). The above shRNA depletion findings mirrored those from CRISPR/Cas9 knockout (KO) of *Il33*, which showed inhibition of tumor growth and a strong reduction in T_H2 infiltration (Figures S3H–S3K). In addition, IL-33 KO produced reductions in other IL-33 responding immunocytes, such as MDSCs and T_{regs}; however, no significant change was observed in $CD8^+$ T cells, neutrophils, and B cell populations (Figures S3L–S3Q). Notably, in addition to the diminished infiltration of ILC2 cells in IL-33-deficient tumors, the activation marker required for ILC2 function, *Tph1* (Flamar et al., 2020) and the effector cytokines, *Il13* and *Il5*, and *Areg* mRNA levels were also reduced, which suggests that the small population of resident ILC2 cells present within the PDAC TME are functionally inactive with decreased IL-33 (Figure 3J). Together, these data establish that cancer-cell-derived IL-33 recruits and activates type 2 immune cells into the PDAC TME.

Intratumor fungi facilitate the secretion of IL-33 from PDAC cells

Immunohistochemistry analysis of PDAC tumors revealed that IL-33 expression was predominantly nuclear in the pre-neoplastic (pancreatic intraepithelial neoplasia 1–3 [PanIN1–3]) and early tumor stages compared with advanced adenocarcinoma when its expression becomes widespread across the cytosol and extracellular milieu (6- versus 24-week-old PDAC

(D) Heatmap of genes enriched in Kras signaling pathway upon comparing Kras ON, OFF-2 days, and OFF-4 days in four murine cell lines.
(E) qRT-PCR analysis of *Il33* expression in the Kras ON, OFF-2 days, and OFF-4 days (n = 3).
(F) Western blot analysis of IL-33 (Lo, low exposure; Hi, high exposure), pERK1/2 (P-p42/44), and ERK1/2 (p42/44) in Kras ON, OFF-1, day, OFF-2 days, and OFF-3 days in the murine cell line.
(G) Western blot analysis of IL-33 and pERK1/2 in Kras ON, OFF, and re-ON in murine cell line.
(H) Western blot analysis of IL-33, pERK1/2 (P-p42/44), and pAkt-S307 upon treatment with MEK inhibitors (CI-1040 and trametinib) in the murine cell line.
(I) Representative confocal images of IL-33 and α-smooth muscle actin (α-SMA) staining in mouse PDAC tumor. Magnification 63×. Scale bars, 50 μm.
(J) Representative immunohistochemistry (IHC) images of IL-33 in human PDAC tumor, with inset (red box) showing 100× magnification (n = 121). Scale bars, 25 μm.
(K) Statistical analysis of IL-33 staining of human PDAC TMA. The intensity of IHC staining was scored as negative (0), low (1), medium (2), and high (3) (left). Right: table showing statistical analysis of the IL-33 expression between normal pancreas and tumor tissues (right). The N-versus-T comparison was done considering all staining (scores 1–3) intensities. See also Figure S2.
Data are presented as mean ± SD. p values were calculated using Student's t test. ns, no significance. Individual p values are indicated in the panels. See also Figure S2.

Please cite this article in press as: Alam et al., Fungal mycobiome drives IL-33 secretion and type 2 immunity in pancreatic cancer, Cancer Cell (2022), https://doi.org/10.1016/j.ccell.2022.01.003

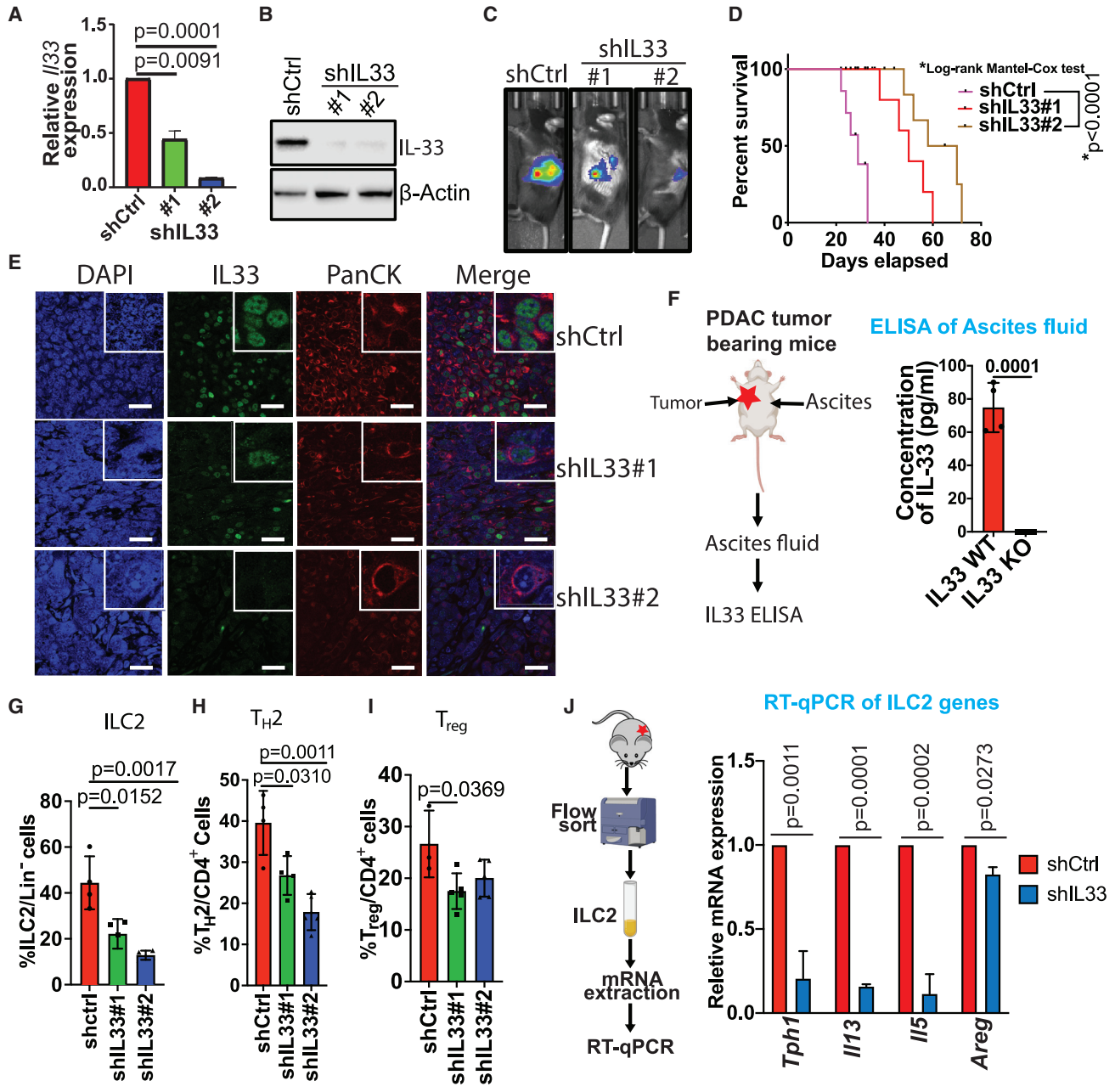

Figure 3. IL-33 is required for recruitment of type 2 immunocytes

(A) *Il33* gene expression was determined by qRT-PCR relative to β-actin in non-target (shCtrl) versus shIL33 (#1 and #2) stable murine cell line (n = 3).

(B) Western blot analysis showing stable knockdown of *Il33* in shIL33 (#1 and #2) murine cell lines. β-Actin was used as a loading control.

(C) Intrapancreatic injection of shCtrl (n = 23) and shIL33 (#1 [n = 25] and #2 [n = 24]) stable PDAC isogenic mouse cell lines. Representative bioluminescence images showing orthotopically transplanted PDAC tumors.

(D) Kaplan-Meier survival curves of mice orthotopically transplanted with shCtrl and shIL33 (#1 and #2) stable PDAC isogenic mouse cell line (n = 10).

(E) Representative confocal images showing cancer-cell-specific nuclear expression of IL-33 (green) in orthotopically transplanted shCtrl and shIL33 PDAC tumors. DAPI (blue) was used as nuclear marker and PanCK (red) as an epithelial cell marker. Magnification 63×. Scale bars, 100 μm.

(F) Schematic showing accumulation of ascites fluid on days 25–28 of orthotopically transplanted shCtrl and shIL33 PDAC tumor-bearing mice (left). IL-33 was quantified in ascites fluid using ELISA (n = 3) (right).

(G) Frequency of ILC2 in orthotopically transplanted shCtrl and shIL33 PDAC tumors relative to total Lin^- cells.

(H) Frequency of T_H2 in orthotopically transplanted shCtrl and shIL33 PDAC tumors relative to total $CD4^+$ cells.

(I) Frequency of T_{reg} in orthotopically transplanted shCtrl and shIL33 PDAC tumors relative to total $CD4^+$ cells.

(J) Schematic showing flow sorting of ILC2 cells from orthotopically transplanted shCtrl and shIL33 PDAC tumors (left). qRT-PCR analysis was performed for ILC2 lineage signature genes *Tph1*, *Il13*, *Il5*, and *Areg* (right).

(legend continued on next page)

Please cite this article in press as: Alam et al., Fungal mycobiome drives IL-33 secretion and type 2 immunity in pancreatic cancer, Cancer Cell (2022), https://doi.org/10.1016/j.ccell.2022.01.003

tumors) (Figure 4A). In contrast, immunofluorescence staining of IL-33 of PDAC cells in culture showed staining primarily in the nucleus (Figure 4B), which was further confirmed by subcellular fractionation studies (Figure 4C). These observations prompted us to consider the possibility that the secretion of IL-33 is regulated by pathways and factors beyond *Kras*^{G12D} signaling that are operative in the TME (Figure S4A). The notion that IL-33 secretion requires an environmental stimulus is further fueled by the fact that IL-33 is a DAMP molecule, and its extracellular secretion is tightly regulated in normal cells to avoid unwanted immune responses (Bonilla et al., 2012; Miller, 2011).

Prior studies in a murine allergic model showed that IL-33 can be secreted by lung epithelial cells in the presence of fungus, thereby exacerbating allergic responses (Snelgrove et al., 2014). Importantly, recent studies reported the presence of intratumor micro- and myco-biome in PDAC, which supports tumor progression (Riquelme et al., 2019; Aykut et al., 2019). As a first step, 18S rRNA sequencing confirmed the presence of mycobiome in our PDAC mouse model (Figures 4D and S4B). Fungal communities were detected in both tumor and gut samples of PDAC-bearing mice and were present in much higher abundance in tumors. *Malassezia* was documented as the most abundant fungi in PDAC tumors. Fluorescence *in situ* hybridization (FISH), which we used to probe for the presence of fungal DNA in the normal pancreas and PDAC tumor, confirmed higher fungal abundance in the PDAC tumor compared with the normal pancreas (Figure 4E).

Next, *in vitro* assays were performed to ascertain the direct role of fungus on IL-33 secretion. We used an array of fungi identified in our 18S rRNA sequencing as well as those reported earlier in PDAC tumors (Aykut et al., 2019). There was a time-course-dependent loss of IL-33 in PDAC cells treated with extracts of *Alternaria alternata* (Figures 4F, 4G, S4C, and S4E), as shown by western blot analysis. The secretion of IL-33 peaks at 3 h after fungal extract treatment and tapers off at 6 h. The secretion completely ceases at about 24 h post treatment. Simultaneously, an ELISA detected IL-33 in the spent medium, which coincides with the loss of IL-33 in cell lysates (Figures 4H, S4D, and S4F). Interestingly, a similar experiment conducted with *Aspergillus* and *Candida* spp. did not yield similar results, indicating that specific fungi species regulate IL-33 secretion in PDAC cells (Figures S4G–S4J). In a separate experiment, cancer cells treated with *A. alternata* showed a time-course-dependent loss of IL-33 as shown by immunofluorescence (Figure S4K).

To determine whether the IL-33 secreted into the spent medium can activate ILC2 cells, we conducted a functional assay whereby we sort-purified ILC2s from mouse spleen and treated the ILC2s with the fungal-treated spent medium from the PDAC cell line (Figure 4I). An ELISA showed robust IL-5 secretion by ILC2 cells (Figure 4J).

Intratumor fungi accelerate PDAC tumor growth

We next assessed the impact of depleting fungi on IL-33 secretion and the type 2 immune response in the PDAC TME. Gastrointestinal fungi in tumor-bearing mice were depleted by oral amphotericin B (anti-fungal) treatment (Figure 5A). Amphotericin B treatment or IL-33 depletion resulted in a significant decrease in tumor burden and increased survival (Figures 5B–5D and S5A–S5C) as well as reduced tumor-infiltrating ILC2 (Figure 5E) and T_H2 cells (Figure 5F).

To further test the role of fungi in IL-33 secretion and recruitment of ILC2 and T_H2 cells in the PDAC TME, we administered *Malassezia globosa* or *A. alternata* by oral gavage to PDAC-bearing mice (Figure 5G). First, fungi resident in the mice were depleted by a course of amphotericin B (i.e., five doses of amphotericin B, 200 μg/day by oral gavage), followed by a maintenance dose of 0.5 μg/mL in the drinking water for 20 days. Following depletion of fungi, we administered either *M. globosa* or *A. alternata* (10^8 fungal spores per mouse) by oral gavage into the tumor-bearing mice. At 28 days after fungal treatment, the tumors were harvested for analyses (Figure S5D). Immunohistochemistry and immunofluorescence showed that fungal-depleted PDAC tumors exhibited an IL-33 signal restricted predominantly to the nucleus of cancer cells, whereas fungi-administered PDAC tumors showed extracellular expression of IL-33 (Figure 5H, top and middle). Intratumoral fungal depletion and repopulation were confirmed by fungal FISH analysis (Figure 5H, bottom). In addition, 18S rRNA sequencing confirmed the increased presence of *Alternaria* and *Malassezia* spp. in the tumor and stool of the mouse receiving fungal transplantation (Figures 5I, S5E, and S5G). Notably, amphotericin B treatment significantly decreased tumor burden, whereas the administration of either *M. globosa* or *A. alternata* promoted tumor growth (Figure 5J). Similarly, *M. globosa* or *A. alternata* administration augmented the infiltration of ILC2 (Figure 5K) and T_H2 (Figure S5H) cell populations within the TME. Moreover, *A. alternata* administration decreased $CD8^+$ T cells, and no significant changes were observed in total $CD4^+$ and B cells (Figures S5I–S5K).

IL-33-mediated ILC2 activation is necessary for tumor progression

To establish a direct link between IL-33-mediated ILC2 activation and tumor progression, we orthotopically co-transplanted ILC2 cells with PDAC cells (Figure 6A). The co-transplantation of PDAC-derived ILC2 cells (donor) into a syngeneic host (recipient) led to a significant increase in tumor burden, while IL-33 KO in cancer cells resulted in significantly reduced tumor burden, which was unaltered with ILC2 co-transplantation (Figures 6B–6E). A complementary experiment demonstrated that retro-orbital injection of ILC2 cells enabled their recruitment to the TME in response to IL-33-expressing PDAC cells. First, to ensure the proper transfer of the retro-orbitally injected ILC2 cells to the PDAC TME, we established a protocol whereby we labeled ILC2 cells with a Vybrant-DiD dye. The DiD-labeled ILC2 cells were then injected retro-orbitally, and 7 days post injection the PDAC tumors were collected and DiD-labeled ILC2 cells were measured by flow cytometry (Figure S6A). The assay confirmed the presence of DiD-labeled ILC2 cells in the PDAC tumor, as

Data are presented as mean ±SD. p values were calculated using Student's t test. ns, no significance. Individual p values are indicated in the panels. See also Figure S3.

Please cite this article in press as: Alam et al., Fungal mycobiome drives IL-33 secretion and type 2 immunity in pancreatic cancer, Cancer Cell (2022), https://doi.org/10.1016/j.ccell.2022.01.003

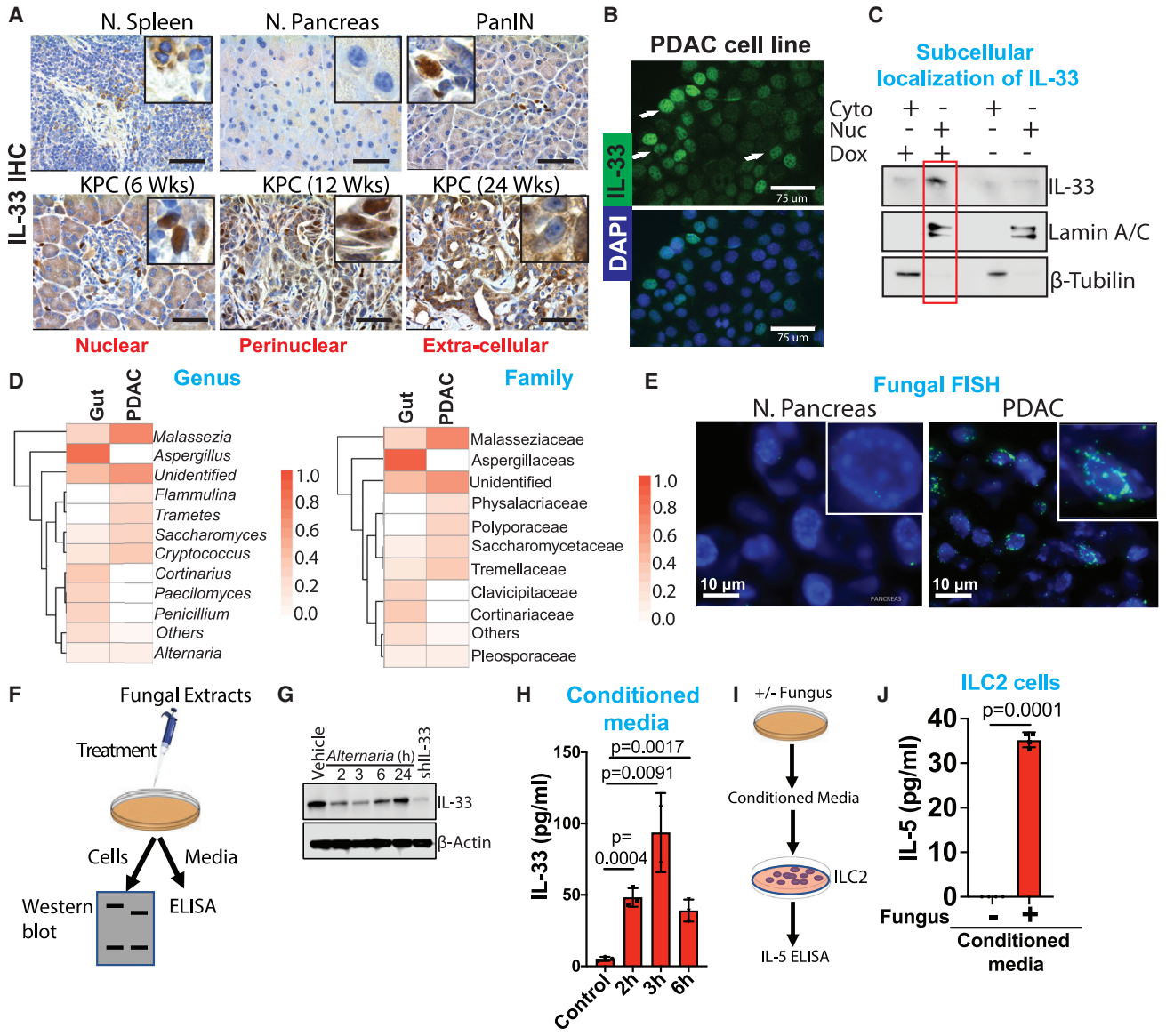

Figure 4. Intratumor fungi facilitate the secretion of IL-33 from PDAC cells

(A) Representative IHC images of IL-33 in the spleen, normal pancreas, PanIN (KC mice), and PDAC (KPC mice) of 6-, 12-, and 24-week-old mice. Scale bars, 50 μm.

(B) Fluorescence images showing nuclear expression of IL-33 (green) in PDAC cell line. DAPI (blue) was used for nuclear staining. Magnification 40×. Scale bars, 75 μm.

(C) Subcellular fractionation of Dox-inducible murine PDAC cell line showing IL-33 expression in cytoplasm and nucleus. Lamin A/C and β-tubulin were used as nuclear and cytoplasmic loading control, respectively.

(D) The gut and intrapancreatic (n = 3, biologically independent samples) mycobiomes of PDAC tumor-bearing mice were analyzed by 18S internal transcribed space (ITS) sequencing. Heatmap shows relative abundance of the fungal genus (left) and family (right) in gut versus PDAC.

(E) Fluorescence *in situ* hybridization (FISH) showing fungal population in normal pancreas versus PDAC. D223 fungal-specific probe was used to detect the fungal species in the normal pancreas.

(F) Schematic showing strategy for fungal extract treatment followed by biochemical assays to determine IL-33 expression in cells and conditioned medium upon treatment with *Alternaria alternata*.

(G) Western blot analysis of IL-33 in PDAC cell line treated with vehicle and fungal extract (*A. alternata*) for different time points (2, 3, 6, and 24 h) and shIL33 PDAC cell line. β-Actin was used as a loading control.

(H) IL-33 was measured in conditioned medium using ELISA in PDAC cell line treated with *A. alternata* extract for different time points (2, 3, and 6 h) (n = 3).

(I) Schematic showing strategy for quantification of IL-5 in flow-sorted ILC2 cells cultured with PDAC cell-conditioned medium treated earlier with the fungal extract.

(J) IL-5 measured using ELISA produced from ILC2s upon treatment with fungal-extract-treated cancer-cell-conditioned medium.

Data are presented as mean ± SD. p values were calculated using Student's t test. ns, no significance. Individual p values are indicated in the panels. See also Figure S4.

Please cite this article in press as: Alam et al., Fungal mycobiome drives IL-33 secretion and type 2 immunity in pancreatic cancer, Cancer Cell (2022), https://doi.org/10.1016/j.ccell.2022.01.003

CellPress

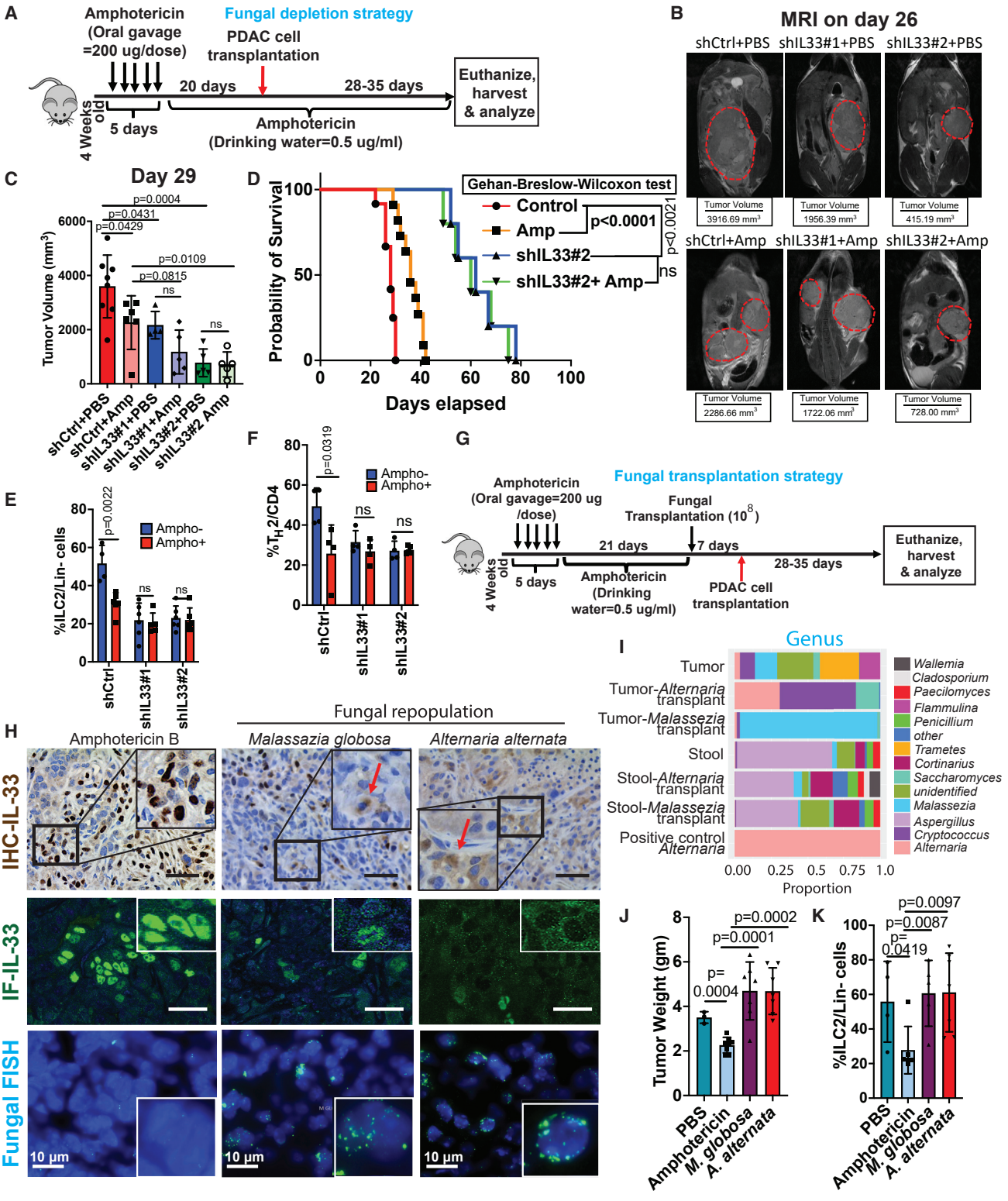

Figure 5. Intratumor fungus accelerates PDAC tumor growth

(A) Schematic showing fungal depletion strategy using amphotericin B (200 µg/dose) followed by orthotopic transplantation of PDAC cells and tumor progression studies.

(B) Representative MRI images with their relative volumes (n = 5) on day 26, showing orthotopically transplanted shCtrl and shIL33 PDAC tumors with or without amphotericin B treatment. Red dotted circles define the tumor boundaries.

(legend continued on next page)

Please cite this article in press as: Alam et al., Fungal mycobiome drives IL-33 secretion and type 2 immunity in pancreatic cancer, Cancer Cell (2022), https://doi.org/10.1016/j.ccell.2022.01.003

shown by the mean fluorescence intensity levels of the ILC2 cells (Figures S6B and S6C). Thereafter, we transplanted ILC2 (1×10^5 cells) into either IL-33 WT or IL-33 KO PDAC-bearing mice. ILC2 transplantation in IL-33-WT mice led to a small increase in tumor growth, whereas IL-33 KO tumors showed minimal change in tumor growth (Figures S6D–S6F).

Prior studies have demonstrated that fungal-derived lectin (e.g., β-glucans) are recognized by a pattern recognition receptor, dectin-1, expressed primarily by macrophages, neutrophils, and DCs. These studies showed that the dectin-1 pathway is involved in the release of cytokines, such as IL-1β, by macrophages (Rosas et al., 2008; Hernanz-Falcon et al., 2009). Thus, to understand the mechanisms governing fungal-mediated IL-33 secretion from PDAC cells, we conducted cell culture studies wherein PDAC cells were exposed to fungal extracts and analyzed for activation of the dectin-1 pathway (Figure 6F). We observed activation of the dectin-1-mediated Src-Syk-CARD9-NFkB pathway, which tracks with the secretion pattern of IL-33 from the PDAC cells (Figures 6G, 6H, and S6G). Of note, dectin-1 is not expressed in normal human pancreatic cells (Figures S6H and S6I). In addition, PDAC tumor-bearing mice treated with amphotericin B showed low expression of CARD9 compared with the untreated tumor-bearing counterparts (Figure 6I). Based on these findings, we conclude that intratumoral fungi or fungal products provoke IL-33 secretion by PDAC cells, which promotes type 2 immune responses and tumor progression (Figure 6J).

DISCUSSION

PDAC tumors are infiltrated by pro-tumorigenic immune cells that include T_H2 and ILC2 cells, which, via their cytokine networks, foster a pro-tumorigenic program that leads to PDAC progression (Mahajan et al., 2018; Liu et al., 2019; Dey et al., 2020; Moral et al., 2020). However, which factors mediate the recruitment and activation of T_H2 and ILC2 cells remains unknown. In this study, we establish that $Kras^{G12D}$ regulates the expression of a chemoattracting cytokine, IL-33, that recruits T_H2 and ILC2 cells. The T_H2 and ILC2 cells via their pro-tumorigenic cytokine production accelerate PDAC tumor progression. Specifically, we established IL-33 as a bona fide downstream target of $Kras^{G12D}$ and that IL-33 expression is significantly upregulated in PDAC patients. We also identified an unanticipated role for the intratumoral mycobiome in facilitating the type 2 immune response in the PDAC TME by stimulating the extracellular secretion of IL-33. This role of intratumor fungus is distinct from prior observation whereby fungi were shown to activate a complement system (Aykut et al., 2019) and might act in tandem to promote PDAC progression. These mechanistic insights governing the extracellular secretion of IL-33 suggest that the IL-33-ILC2/T_H2 axis is a potential target in PDAC. Accordingly, in a preclinical proof-of-concept study, genetic deficiency of IL-33 or an anti-fungal treatment decreased tumor burden and prolonged survival in mice.

Although the definitive molecular link between fungal components and IL-33 secretion remains to be identified, our study has revealed an important connection between the intratumoral mycobiome and the spatiotemporal secretion of IL-33 in the PDAC TME. We found that fungal-derived components can activate a dectin-1-dependent pathway, reminiscent of similar fungal response pathways observed in macrophages and DCs. Specifically, fungi can activate a dectin-1-mediated Src-Syk-CARD9 pathway which, via downstream mechanisms, secretes IL-33. In addition to fungi, biochemical factors, such as reactive oxygen species and oxidative stress (Taniguchi et al., 2020; Uchida et al., 2017), can promote the extracellular secretion of IL-33. These factors might act in concert with the mycobiome as a stimulator and amplifier of IL-33 secretion. Notably, we and others have found that fungal components can be detected in the early stages of PDAC tumorigenesis, such as in PanIN (Aykut et al., 2019) when a large-scale oxidative stress has yet to be detected in the TME. This raises the question of whether the mycobiome is responsible for initiating the type 2 immune response in PDAC, which is further reinforced by factors such as oxidative stress and other yet to be discovered processes or vice versa.

Recent studies using metagenomic sequencing have demonstrated the presence of intratumoral fungi in PDAC (Aykut et al., 2019). A possible route for microbial migration from the duodenum to the pancreas is the retrograde transfer via the opening of the sphincter of Oddi, which controls the flow of digestive juices (bile and pancreatic) from the pancreas and gall bladder. We have validated this finding in our mouse model where we found that PDAC tumors are infiltrated mostly by fungal genera such as *Alternaria* and *Malassezia*. The question is how early in the PDAC tumorigenesis process does this retrograde transfer of fungi occur. The chain of events is crucial to understanding the

(C) Bar graph showing tumor volume of orthotopically transplanted shCtrl and shIL33 PDAC tumors (n = 14) and shIL33 (#1 [n = 9] and #2 [n = 10]) with or without amphotericin B treatment.
(D) Kaplan-Meier survival curves of mice orthotopically transplanted with shCtrl and shIL33 PDAC tumors with or without amphotericin B treatment (n = 10). Statistical analysis was done using the Gehan-Breslow Wilcoxon test.
(E) Frequency of ILC2 in orthotopically transplanted shCtrl and shIL33 PDAC tumors with or without amphotericin B treatment relative to total Lin^- cells.
(F) Frequency of T_H2 cells in orthotopically transplanted shCtrl and shIL33 PDAC tumors with or without amphotericin B treatment relative to total $CD4^+$ cells.
(G) Schematic showing strategy for fungal transplantation followed by orthotopic transplantation of PDAC cells and tumor progression studies.
(H) Representative IHC (top) and immunofluorescence (middle) images of PDAC tumors showing IL-33 expression in control and fungal transplanted mice by oral gavage (n = 10). Magnification 40×. Scale bars, 100 μm. Bottom: FISH showing fungal colonization of PDAC tumors in fungal transplanted mice by oral gavage. Scale bars, 10 μm.
(I) 18S rRNA sequence showing fungal species in PDAC tumors of the *A. alternata* and *Malassezia globosa* transplanted mice by oral gavage. Also shown are the 18S rRNA sequencing in stool samples of the *A. alternata* and *M. globosa* transplanted mice by oral gavage. Positive control *Alternaria* is a sample of pure *A. alternata* culture extract.
(J) Bar graph showing the wet weight of PDAC tumors of the control, amphotericin B, and fungal transplanted mice (n = 10).
(K) Frequency of ILC2/total Lin^- cells in PDAC tumors of control, amphotericin B, and fungal transplanted mice.
Data are presented as mean ± SD. p values were calculated using Student's t test. ns, no significance. Individual p values are indicated in the panels. See also Figure S5.

Please cite this article in press as: Alam et al., Fungal mycobiome drives IL-33 secretion and type 2 immunity in pancreatic cancer, Cancer Cell (2022), https://doi.org/10.1016/j.ccell.2022.01.003

CellPress

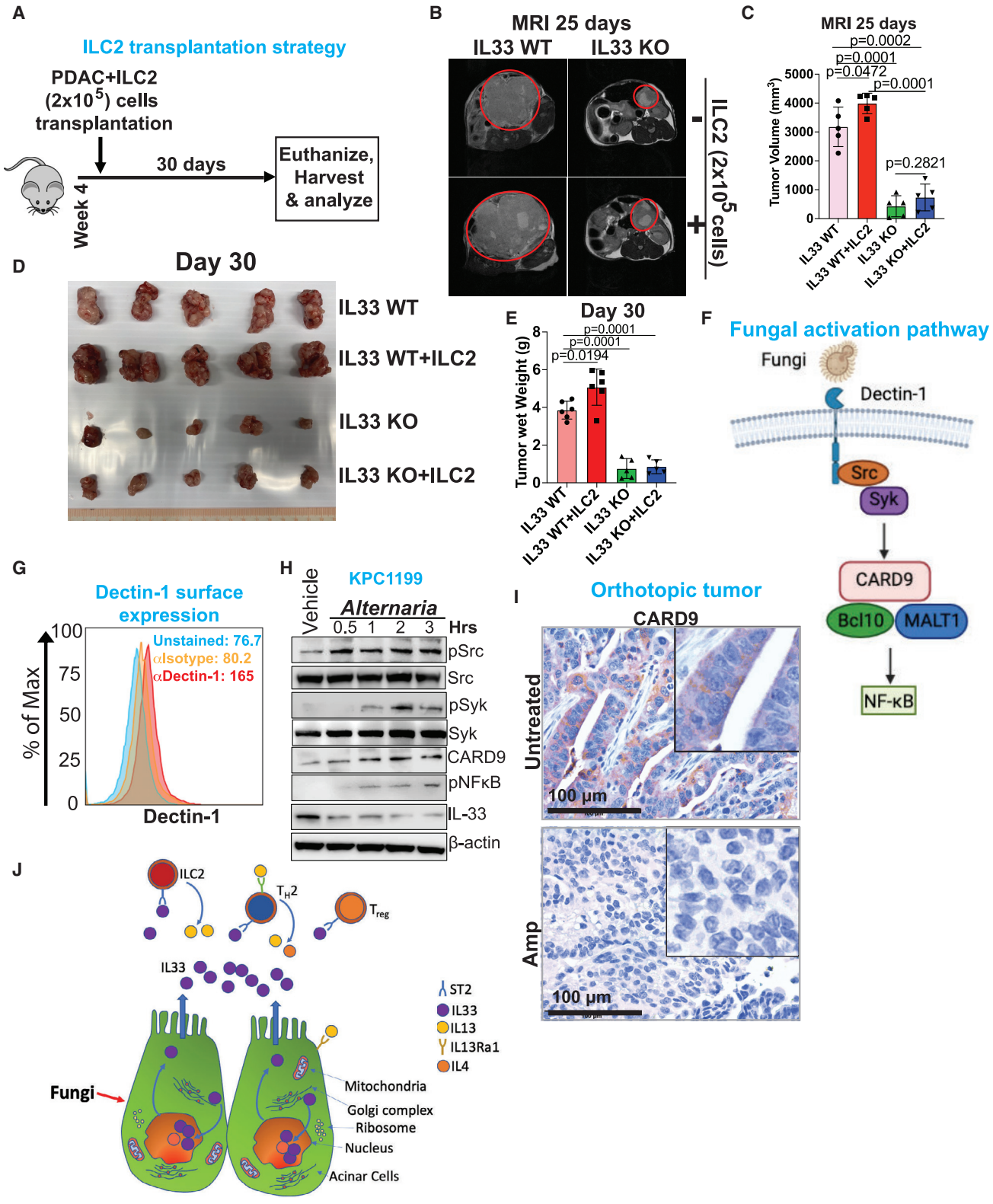

Figure 6. IL-33-mediated ILC2 activation is necessary for tumor progression

Figure360▷ For a Figure360 author presentation of Figure 6J, see https://doi.org/10.1016/j.ccell.2022.01.003#mmc2.

(A) Schematic showing strategy for orthotopic co-transplantation of PDAC and ILC2 cells.

(B) Representative MRI scans showing axial images of CRISPR/Cas9 knockout tumors (IL-33 WT versus IL-33 KO), with or without ILC2 co-transplantation.

(legend continued on next page)

Please cite this article in press as: Alam et al., Fungal mycobiome drives IL-33 secretion and type 2 immunity in pancreatic cancer, Cancer Cell (2022), https://doi.org/10.1016/j.ccell.2022.01.003

mechanism of IL-33 secretion into the extracellular space, the recruitment and activation of ILC2 and T_H2 cells, and the secretion of pro-tumorigenic cytokines. In addition to the intratumor fungal microbiome, the role of the bacterial microbiome as a collaborator cannot be ruled out, as studies have shown that Gram-negative bacteria can stimulate IL-33 secretion in the nasopharynx (Hentschke et al., 2017). Recent studies have also demonstrated the presence of intratumor bacterial microbiome in PDAC models, and consequent antibiotic treatment reduces tumor growth, increases M1-type macrophage abundance, promotes T_H1 differentiation, and stimulates $CD8^+$ T cell activation (Riquelme et al., 2019).

Although IL-33 plays a predominant role in PDAC progression, as its deletion leads to significant tumor regression and increased survival, the role of IL-33 is context dependent and sometimes has opposite effects in various cancer types. Moreover, IL-33 is involved in a myriad of functions depending on the spatial context of the protein. For example, the immune function of IL-33 described here is distinct from its cancer-cell-intrinsic function that has been described recently, whereby IL-33 mediates a pancreas tissue injury program in Kras mutant mice (Park et al., 2021; Alonso-Curbelo et al., 2021). Importantly, IL-33 has been shown to cooperate with mutant Kras to initiate pancreatic neoplasia by a chromatin switch (Alonso-Curbelo et al., 2021).

Given the divergent function of ILC2s in different tumor types and also the context-dependent role of ILC2 in tumor progression, further study is necessary to tease apart the role of ILC2 cells in PDAC and other cancers. For example, mice lacking the IL-33 receptor ST2 have slower tumor progression by increasing T_H1 and natural killer cell activity, hinting toward a pro-tumorigenic role of an IL-33-ILC2 axis (Jovanovic et al., 2011; Ercolano et al., 2019). In contrast, a recent study found that ILC2 infiltration in PDAC cells positively correlates with long-time survival in patients (Moral et al., 2020). According to that study, the infiltrating ILC2 cells are anti-tumorigenic due to their ability to engage $CD103^+$ DCs, while PD-1 expression constrains the anti-tumor activity of ILC2 cells; thus, anti-PD-1 plus recombinant IL-33 (rIL-33) should provide clinical benefit. The stark contrast between this and our study can be explained at various levels. First, the study focused exclusively on the ILC2-$CD103^+$ DC-$CD8^+$ T cell axis, although the main effector cytokines of ILC2 cells are IL-4 and IL-13, which are potent inducers of M2-like macrophage polarization and are central players in immune suppression in the PDAC TME (Zhu et al., 2017). Second, our study and those of other investigators showed that oncogenic KRAS and/or tissue damage (Alonso-Curbelo et al., 2021; Park et al., 2021) already potently upregulates IL-33 expression in PDAC, raising uncertainty as to the utility of injecting rIL-33 as a treatment regimen for PDAC. Finally, the tumor models used in the study induced a robust $CD8^+$ T cell response, which contrasts with the poorly immunogenic PDAC models used in our study, suggesting that IL-33 may have different outcomes in immunogenic tumors that are capable of priming endogenous anti-tumor $CD8^+$ T cells.

Finally, while anti-fungal treatment may appear to be an attractive therapeutic option for PDAC; our *in vivo* studies show that anti-fungal treatment might be insufficient to inhibit IL-33 secretion and suppress tumor growth. It is possible that fungal components as opposed to live fungus are sufficient for IL-33 secretion as demonstrated by our *in vitro* studies. Along these lines, it is worth noting that our attempts to culture live fungus from fresh tumor samples have been unsuccessful to date. This may relate to a lack of live fungus or phagocytic elimination of fungus by intratumoral macrophages which, in turn, release fungal components such as chitin, β-glucans, and DNA/RNA fragments into the PDAC TME. Thus, the absence of live fungi would render anti-fungal treatment inconsequential in a prolonged treatment paradigm. Alternatively, it is possible that live fungi are present, but we are unable to culture the fungi because >75% of the microbiome is not culturable using conventional culturing techniques (Watterson et al., 2020), albeit efforts are being made to improve such culturing methodologies. Nevertheless, the fungal components are crucial for regulating an integral pro-tumorigenic cancer-immune cell axis which, if targeted, can yield potentially significant benefit to PDAC patients.

Finally, it is likely that ILC2 plays a variable role in the early and late stages of the tumorigenesis. Seen in this light, the effects of fungi in priming the IL-33-ILC2 axis may have different consequences based on the tumor type, location, and extent of tumor burden, while the involvement of fungi adds another layer of complexity to the IL-33-ILC2 axis.

STAR★METHODS

Detailed methods are provided in the online version of this paper and include the following:

- KEY RESOURCES TABLE
- RESOURCE AVAILABILITY
  - Lead contact
  - Materials availability
  - Data and code availability
- EXPERIMENTAL MODEL AND SUBJECT DETAILS
  - Ethics statement and animal modeling
  - Human PDAC primary tumor samples
  - Mice and tumor models
- METHOD DETAILS
  - *In vivo* imaging
  - Transcriptomic profiling by RNA-seq and qRT-PCR

(C) Bar graph showing tumor volume calculated by MRI image analysis (n = 5–7).
(D) Picture showing gross PDAC tumor with or without ILC2 in IL-33 WT versus IL-33 KO mice (n = 5).
(E) Bar graph showing PDAC tumor wet weight with or without ILC2 in IL-33 WT versus IL-33 KO mice (n = 5–7).
(F) Schematic showing fungal activation pathway, where dectin-1 receptor ligates fungal components and induces Src-Syk-CARD9 signaling cascade.
(G) Histogram showing dectin-1 expression on PDAC cell line, analyzed by flow cytometry (n = 3).
(H) Western blot showing expression of pSrc, Src, pSyk, Syk, CARD9, p-NFκB, and IL-33 upon treatment with *A. alternata*. β-Actin was used as a loading control.
(I) Representative IHC image showing CARD9 expression in orthotopic transplanted tumor with or without anti-fungal treatment. Scale bars, 100 μm.
(J) Working model showing fungus-mediated secretion of IL-33 from PDAC tumor, attracting type 2 immune cells (ILC2, T_H2, and T_{reg}), thereby promoting tumor progression.
Results are shown as mean ± SD. p values were calculated using Student's t test. Individual p values are indicated in the panels. See also Figure S6.

- Single cell RNA sequencing (scRNAseq)
- Flow cytometry
- Immunoblotting and antibodies
- Immunohistochemistry and immunofluorescence
- Cell culture and establishment of primary PDAC lines
- shRNA and CRISPR-Cas9 knockdown
- Anti-fungal treatment and fungal challenge experiments
- Fungal fluorescence in situ hybridization (FISH)
- 18S rRNA sequencing and mycobiome analysis
- Enzyme linked immunosorbent assay (ELISA)
- ILC2 enrichment and adoptive transfer of ILC2
- ILC2 Co-transplantation

- QUANTIFICATION AND STATISTICAL ANALYSIS
  - Statistical analysis

SUPPLEMENTAL INFORMATION

Supplemental information can be found online at https://doi.org/10.1016/j.ccell.2022.01.003.

ACKNOWLEDGMENTS

We thank the Roswell Park core facilities supported by the National Cancer Institute (NCI) grant P30CA016056, including Genomic, Bioinformatics and Biostatistics, Data Bank and repository, Pathology Network, and Flow and Imaging Cytometry shared resources. In addition, this study was supported by 5R00CA218891-04 (P.D.), 1R01CA262822-01 (P.D.), The Roswell Park Alliance Foundation, United States-62-2839-01 (P.D.), R01CA188900 (B.I.S.), R01CA172105 (S.I.A.), P01CA234212 (P.K.), R01CA218004 (A.M.) and Sheikh Khalifa Bin Zayed Foundation, United States (A.M.), R01CA196941 (H.W.), R01CA195651 (H.W.), P01CA117969 (R.A.D.), R01CA225955 (R.A.D.), and the Burkhart III Distinguished University Chair in Cancer Research Endowment (R.A.D.). We thank Dr. Michael Feigin for sharing the KPC1199 cell line. We also thank Dr. Shyamananda Singh Mayengbam for his technical support during revision. Graphical abstract was created with BioRender.com.

AUTHOR CONTRIBUTIONS

Conceptualization, P. Dey; methodology, A.A. and P. Dey; investigation, A.A., E.L., P. Denz, H.S.V., M.B., L.A., S.G.T., Y.Z., E.C.G., J.W., P.K.S., J.L., B.M., S.A., S.S., S.J.S., H.W., and W.L.; writing – original draft, P. Dey; writing – review & editing, P. Dey, A.M., P.K., B.H.S., S.I.A., and R.A.D.; funding acquisition, P. Dey; Supervision, P. Dey.

DECLARATION OF INTERESTS

P. Dey and A.A. have a patent pending on targeting IL-33 and mycobiome in cancer: US Provisional Patent Application Serial No. 63/238,531. R.A.D. is a co-founder, adviser, and/or director of Tvardi Therapeutics, Asylia Therapeutics, Stellanova Therapeutics, Nirogy Therapeutics, and Sporos Bioventures. Tvardi and Nirogy are developing STAT3 and MCT inhibitors, respectively. A.M. receives royalties from Cosmos Wisdom Biotechnology and Thrive Earlier Detection, an Exact Sciences Company. A.M. is also a consultant for Freenome and Tezcat Biotechnology. The other authors declare no competing interests.

INCLUSION AND DIVERSITY

One or more of the authors of this paper self-identifies as a member of the LGBTQ+ community. One or more of the authors of this paper self-identifies as an underrepresented ethnic minority in science.

Received: May 6, 2021
Revised: October 30, 2021
Accepted: January 6, 2022
Published: February 3, 2022

SUPPORTING CITATIONS

The following references appear in the supplemental information: Uhlen et al. (2015); Uhlen et al. (2017).

REFERENCES

Abarenkov, K., Nilsson, H.R., Larsson, K.H., Alexander, I.J., Eberhardt, U., Erland, S., Hoiland, K., Kjoller, R., Larsson, E., Pennanen, T., et al. (2010). The UNITE database for molecular identification of fungi—recent updates and future perspectives. New Phytol. *186*, 281–285.

Aguirre, A.J., Bardeesy, N., Sinha, M., Lopez, L., Tuveson, D.A., Horner, J., Redston, M.S., and Depinho, R.A. (2003). Activated Kras and Ink4a/Arf deficiency cooperate to produce metastatic pancreatic ductal adenocarcinoma. Genes Dev. *17*, 3112–3126.

Alamri, A., Nam, J.Y., and Blancato, J.K. (2017). Fluorescence in situ hybridization of cells, chromosomes, and formalin-fixed paraffin-embedded tissues. Methods Mol. Biol. *1606*, 265–279.

Ali, S., Huber, M., Kollewe, C., Bischoff, S.C., Falk, W., and Martin, M.U. (2007). IL-1 receptor accessory protein is essential for IL-33-induced activation of T lymphocytes and mast cells. Proc. Natl. Acad. Sci. U.S.A *104*, 18660–18665.

Alonso-Curbelo, D., Ho, Y.J., Burdziak, C., Maag, J.L.V., Morris, J.P.T., Chandwani, R., Chen, H.A., Tsanov, K.M., Barriga, F.M., Luan, W., et al. (2021). A gene-environment-induced epigenetic program initiates tumorigenesis. Nature *590*, 642–648.

Anders, S., Pyl, P.T., and Huber, W. (2015). HTSeq—a Python framework to work with high-throughput sequencing data. Bioinformatics *31*, 166–169.

Aran, D., Looney, A.P., Liu, L., Wu, E., Fong, V., Hsu, A., Chak, S., Naikawadi, R.P., Wolters, P.J., Abate, A.R., et al. (2019). Reference-based analysis of lung single-cell sequencing reveals a transitional profibrotic macrophage. Nat. Immunol. *20*, 163–172.

Aykut, B., Pushalkar, S., Chen, R., Li, Q., Abengozar, R., Kim, J.I., Shadaloey, S.A., Wu, D., Preiss, P., Verma, N., et al. (2019). The fungal mycobiome promotes pancreatic oncogenesis via activation of MBL. Nature *574*, 264–267.

Bonilla, W.V., Frohlich, A., Senn, K., Kallert, S., Fernandez, M., Johnson, S., Kreutzfeldt, M., Hegazy, A.N., Schrick, C., Fallon, P.G., et al. (2012). The alarmin interleukin-33 drives protective antiviral CD8(+) T cell responses. Science *335*, 984–989.

Caporaso, J.G., Kuczynski, J., Stombaugh, J., Bittinger, K., Bushman, F.D., Costello, E.K., Fierer, N., Pena, A.G., Goodrich, J.K., Gordon, J.I., et al. (2010). QIIME allows analysis of high-throughput community sequencing data. Nat. Methods *7*, 335–336.

Clark, C.E., Hingorani, S.R., Mick, R., Combs, C., Tuveson, D.A., and Vonderheide, R.H. (2007). Dynamics of the immune reaction to pancreatic cancer from inception to invasion. Cancer Res. *67*, 9518–9527.

Cui, G., Yuan, A., Pang, Z., Zheng, W., Li, Z., and Goll, R. (2018). Contribution of IL-33 to the pathogenesis of colorectal cancer. Front. Oncol. *8*, 561.

De Monte, L., Reni, M., Tassi, E., Clavenna, D., Papa, I., Recalde, H., Braga, M., Di Carlo, V., Doglioni, C., and Protti, M.P. (2011). Intratumor T helper type 2 cell infiltrate correlates with cancer-associated fibroblast thymic stromal lymphopoietin production and reduced survival in pancreatic cancer. J. Exp. Med. *208*, 469–478.

Dey, P., Baddour, J., Muller, F., Wu, C.C., Wang, H., Liao, W.T., Lan, Z., Chen, A., Gutschner, T., Kang, Y., et al. (2017). Genomic deletion of malic enzyme 2 confers collateral lethality in pancreatic cancer. Nature *542*, 119–123.

Dey, P., Jonsson, P., Hartman, J., Williams, C., Strom, A., and Gustafsson, J.A. (2012). Estrogen receptors beta1 and beta2 have opposing roles in regulating proliferation and bone metastasis genes in the prostate cancer cell line PC3. Mol. Endocrinol. *26*, 1991–2003.

Dey, P., Li, J., Zhang, J., Chaurasiya, S., Strom, A., Wang, H., Liao, W.T., Cavallaro, F., Denz, P., Bernard, V., et al. (2020). Oncogenic KRAS-driven metabolic reprogramming in pancreatic cancer cells utilizes cytokines from the tumor microenvironment. Cancer Discov. *10*, 608–625.

Dey, P., Strom, A., and Gustafsson, J.A. (2014). Estrogen receptor beta upregulates FOXO3a and causes induction of apoptosis through PUMA in prostate cancer. Oncogene *33*, 4213–4225.

Dobin, A., Davis, C.A., Schlesinger, F., Drenkow, J., Zaleski, C., Jha, S., Batut, P., Chaisson, M., and Gingeras, T.R. (2013). STAR: ultrafast universal RNA-seq aligner. Bioinformatics *29*, 15–21.

Ercolano, G., Falquet, M., Vanoni, G., Trabanelli, S., and Jandus, C. (2019). ILC2s: new actors in tumor immunity. Front. Immunol. *10*, 2801.

Feig, C., Gopinathan, A., Neesse, A., Chan, D.S., Cook, N., and Tuveson, D.A. (2012). The pancreas cancer microenvironment. Clin. Cancer Res. *18*, 4266–4276.

Flamar, A.L., Klose, C.S.N., Moeller, J.B., Mahlakoiv, T., Bessman, N.J., Zhang, W., Moriyama, S., Stokic-Trtica, V., Rankin, L.C., Putzel, G.G., et al. (2020). Interleukin-33 induces the enzyme tryptophan hydroxylase 1 to promote inflammatory group 2 innate lymphoid cell-mediated immunity. Immunity *52*, 606–619.e6.

Fournie, J.J., and Poupot, M. (2018). The pro-tumorigenic IL-33 involved in antitumor immunity: a Yin and Yang cytokine. Front. Immunol. *9*, 2506.

Gopalakrishnan, V., Spencer, C.N., Nezi, L., Reuben, A., Andrews, M.C., Karpinets, T.V., Prieto, P.A., Vicente, D., Hoffman, K., Wei, S.C., et al. (2018). Gut microbiome modulates response to anti-PD-1 immunotherapy in melanoma patients. Science *359*, 97–103.

Hao, Y., Hao, S., Andersen-Nissen, E., Mauck, W.M., 3rd, Zheng, S., Butler, A., Lee, M.J., Wilk, A.J., Darby, C., Zager, M., et al. (2021). Integrated analysis of multimodal single-cell data. Cell *184*, 3573–3587.e29.

Hentschke, I., Graser, A., Melichar, V.O., Kiefer, A., Zimmermann, T., Kross, B., Haag, P., Xepapadaki, P., Papadopoulos, N.G., Bogdan, C., and Finotto, S. (2017). IL-33/ST2 immune responses to respiratory bacteria in pediatric asthma. Sci. Rep. *7*, 43426.

Hernanz-Falcon, P., Joffre, O., Williams, D.L., and Reis E Sousa, C. (2009). Internalization of dectin-1 terminates induction of inflammatory responses. Eur. J. Immunol. *39*, 507–513.

Hingorani, S.R., Petricoin, E.F., Maitra, A., Rajapakse, V., King, C., Jacobetz, M.A., Ross, S., Conrads, T.P., Veenstra, T.D., Hitt, B.A., et al. (2003). Preinvasive and invasive ductal pancreatic cancer and its early detection in the mouse. Cancer Cell *4*, 437–450.

Jovanovic, I., Radosavljevic, G., Mitrovic, M., Juranic, V.L., Mckenzie, A.N., Arsenijevic, N., Jonjic, S., and Lukic, M.L. (2011). ST2 deletion enhances innate and acquired immunity to murine mammary carcinoma. Eur. J. Immunol. *41*, 1902–1912.

Koljalg, U., Nilsson, R.H., Abarenkov, K., Tedersoo, L., Taylor, A.F., Bahram, M., Bates, S.T., Bruns, T.D., Bengtsson-Palme, J., Callaghan, T.M., et al. (2013). Towards a unified paradigm for sequence-based identification of fungi. Mol. Ecol. *22*, 5271–5277.

Li, A., Herbst, R.H., Canner, D., Schenkel, J.M., Smith, O.C., Kim, J.Y., Hillman, M., Bhutkar, A., Cuoco, M.S., Rappazzo, C.G., et al. (2019). IL-33 signaling alters regulatory T cell diversity in support of tumor development. Cell Rep. *29*, 2998–3008.e8.

Liew, F.Y., Girard, J.P., and Turnquist, H.R. (2016). Interleukin-33 in health and disease. Nat. Rev. Immunol. *16*, 676–689.

Lingel, A., Weiss, T.M., Niebuhr, M., Pan, B., Appleton, B.A., Wiesmann, C., Bazan, J.F., and Fairbrother, W.J. (2009). Structure of IL-33 and its interaction with the ST2 and IL-1RAcP receptors—insight into heterotrimeric IL-1 signaling complexes. Structure *17*, 1398–1410.

Liu, X., Xu, J., Zhang, B., Liu, J., Liang, C., Meng, Q., Hua, J., Yu, X., and Shi, S. (2019). The reciprocal regulation between host tissue and immune cells in pancreatic ductal adenocarcinoma: new insights and therapeutic implications. Mol Cancer *18*, 184, 41.

Mahajan, U.M., Langhoff, E., Goni, E., Costello, E., Greenhalf, W., Halloran, C., Ormanns, S., Kruger, S., Boeck, S., Ribback, S., Beyer, G., et al. (2018). Immune cell and stromal signature associated with progression-free survival of patients with resected pancreatic ductal adenocarcinoma. Gastroenterology *155*, 1625-1639.e2.

Matson, V., Fessler, J., Bao, R., Chongsuwat, T., Zha, Y., Alegre, M.L., Luke, J.J., and Gajewski, T.F. (2018). The commensal microbiome is associated with anti-PD-1 efficacy in metastatic melanoma patients. Science *359*, 104–108.

Mcmurdie, P.J., and Holmes, S. (2013). phyloseq: an R package for reproducible interactive analysis and graphics of microbiome census data. PLoS One *8*, e61217.

Miller, A.M. (2011). Role of IL-33 in inflammation and disease. J. Inflamm. *8*, 22.

Moral, J.A., Leung, J., Rojas, L.A., Ruan, J., Zhao, J., Sethna, Z., Ramnarain, A., Gasmi, B., Gururajan, M., Redmond, D., et al. (2020). ILC2s amplify PD-1 blockade by activating tissue-specific cancer immunity. Nature *579*, 130–135.

Oksanen, J., Kindt, R., Legendre, P., O'Hara, B., Stevens, H.H., and Wagner, H. (2007). The Vegan Package. Community Ecology Package (The R Foundation).

Olive, K.P., Tuveson, D.A., Ruhe, Z.C., Yin, B., Willis, N.A., Bronson, R.T., Crowley, D., and Jacks, T. (2004). Mutant p53 gain of function in two mouse models of Li-Fraumeni syndrome. Cell *119*, 847–860.

Park, J.H., Ameri, A.H., Dempsey, K.E., Conrad, D.N., Kem, M., Mino-Kenudson, M., and Demehri, S. (2021). Nuclear IL-33/SMAD signaling axis promotes cancer development in chronic inflammation. EMBO J. *40*, e106151.

Pastille, E., Wasmer, M.H., Adamczyk, A., Vu, V.P., Mager, L.F., Phuong, N.N.T., Palmieri, V., Simillion, C., Hansen, W., Kasper, S., et al. (2019). The IL-33/ST2 pathway shapes the regulatory T cell phenotype to promote intestinal cancer. Mucosal Immunol. *12*, 990–1003.

Piro, G., Simionato, F., Carbone, C., Frizziero, M., Malleo, G., Zanini, S., Casolino, R., Santoro, R., Mina, M.M., Zecchetto, C., et al. (2017). A circulating TH2 cytokines profile predicts survival in patients with resectable pancreatic adenocarcinoma. Oncoimmunology *6*, e1322242.

Rank, M.A., Kobayashi, T., Kozaki, H., Bartemes, K.R., Squillace, D.L., and Kita, H. (2009). IL-33-activated dendritic cells induce an atypical TH2-type response. J. Allergy Clin. Immunol. *123*, 1047–1054.

Riquelme, E., Zhang, Y., Zhang, L., Montiel, M., Zoltan, M., Dong, W., Quesada, P., Sahin, I., Chandra, V., San Lucas, A., et al. (2019). Tumor microbiome diversity and composition influence pancreatic cancer outcomes. Cell *178*, 795–806.e12.

Robinette, M.L., Fuchs, A., Cortez, V.S., Lee, J.S., Wang, Y., Durum, S.K., Gilfillan, S., Colonna, M., and Immunological Genome, C. (2015). Transcriptional programs define molecular characteristics of innate lymphoid cell classes and subsets. Nat. Immunol. *16*, 306–317.

Robinson, M.D., Mccarthy, D.J., and Smyth, G.K. (2010). edgeR: a Bioconductor package for differential expression analysis of digital gene expression data. Bioinformatics *26*, 139–140.

Rognes, T., Flouri, T., Nichols, B., Quince, C., and Mahe, F. (2016). VSEARCH: a versatile open source tool for metagenomics. PeerJ *4*, e2584.

Rosas, M., Liddiard, K., Kimberg, M., Faro-Trindade, I., Mcdonald, J.U., Williams, D.L., Brown, G.D., and Taylor, P.R. (2008). The induction of inflammation by dectin-1 in vivo is dependent on myeloid cell programming and the progression of phagocytosis. J. Immunol. *181*, 3549–3557.

Schmitz, J., Owyang, A., Oldham, E., Song, Y., Murphy, E., Mcclanahan, T.K., Zurawski, G., Moshrefi, M., Qin, J., Li, X., et al. (2005). IL-33, an interleukin-1-like cytokine that signals via the IL-1 receptor-related protein ST2 and induces T helper type 2-associated cytokines. Immunity *23*, 479–490.

Snelgrove, R.J., Gregory, L.G., Peiro, T., Akthar, S., Campbell, G.A., Walker, S.A., and Lloyd, C.M. (2014). *Alternaria*-derived serine protease activity drives IL-33-mediated asthma exacerbations. J. Allergy Clin. Immunol. *134*, 583–592.e6.

Steele, C.W., Jamieson, N.B., Evans, T.R., Mckay, C.J., Sansom, O.J., Morton, J.P., and Carter, C.R. (2013). Exploiting inflammation for therapeutic gain in pancreatic cancer. Br. J. Cancer *108*, 997–1003.

Taniguchi, S., Elhance, A., Van Duzer, A., Kumar, S., Leitenberger, J.J., and Oshimori, N. (2020). Tumor-initiating cells establish an IL-33-TGF-beta niche signaling loop to promote cancer progression. Science *369*, eaay1813.

Tibbitt, C.A., Stark, J.M., Martens, L., Ma, J., Mold, J.E., Deswarte, K., Oliynyk, G., Feng, X., Lambrecht, B.N., De Bleser, P., et al. (2019). Single-cell RNA

sequencing of the T helper cell response to house dust mites defines a distinct gene expression signature in airway Th2 cells. Immunity *51*, 169–184.e5.

Uchida, M., Anderson, E.L., Squillace, D.L., Patil, N., Maniak, P.J., Iijima, K., Kita, H., and O'grady, S.M. (2017). Oxidative stress serves as a key checkpoint for IL-33 release by airway epithelium. Allergy *72*, 1521–1531.

Uhlen, M., Fagerberg, L., Hallstrom, B.M., Lindskog, C., Oksvold, P., Mardinoglu, A., Sivertsson, A., Kampf, C., Sjostedt, E., Asplund, A., et al. (2015). Proteomics. Tissue-based map of the human proteome. Science *347*, 1260419.

Uhlen, M., Zhang, C., Lee, S., Sjostedt, E., Fagerberg, L., Bidkhori, G., Benfeitas, R., Arif, M., Liu, Z., Edfors, F., et al. (2017). A pathology atlas of the human cancer transcriptome. Science *357*, eaan2507.

Van Gool, F., Molofsky, A.B., Morar, M.M., Rosenzwajg, M., Liang, H.E., Klatzmann, D., Locksley, R.M., and Bluestone, J.A. (2014). Interleukin-5-producing group 2 innate lymphoid cells control eosinophilia induced by interleukin-2 therapy. Blood *124*, 3572–3576.

Venmar, K.T., Kimmel, D.W., Cliffel, D.E., and Fingleton, B. (2015). IL4 receptor alpha mediates enhanced glucose and glutamine metabolism to support breast cancer growth. Biochim. Biophys. Acta *1853*, 1219–1228.

Vivier, E., Artis, D., Colonna, M., Diefenbach, A., Di Santo, J.P., Eberl, G., Koyasu, S., Locksley, R.M., Mckenzie, A.N.J., Mebius, R.E., et al. (2018). Innate lymphoid cells: 10 years on. Cell *174*, 1054–1066.

Wang, K., Shan, S., Yang, Z., Gu, X., Wang, Y., Wang, C., and Ren, T. (2017). IL-33 blockade suppresses tumor growth of human lung cancer through direct and indirect pathways in a preclinical model. Oncotarget *8*, 68571–68582.

Watterson, W.J., Tanyeri, M., Watson, A.R., Cham, C.M., Shan, Y., Chang, E.B., Eren, A.M., and Tay, S. (2020). Droplet-based high-throughput cultivation for accurate screening of antibiotic resistant gut microbes. eLife *9*, e56998.

Ying, H., Dey, P., Yao, W., Kimmelman, A.C., Draetta, G.F., Maitra, A., and Depinho, R.A. (2016). Genetics and biology of pancreatic ductal adenocarcinoma. Genes Dev. *30*, 355–385.

Ying, H., Kimmelman, A.C., Lyssiotis, C.A., Hua, S., Chu, G.C., Fletcher-Sananikone, E., Locasale, J.W., Son, J., Zhang, H., Coloff, J.L., et al. (2012). Oncogenic Kras maintains pancreatic tumors through regulation of anabolic glucose metabolism. Cell *149*, 656–670.

Zervos, E.E., Osborne, D., Boe, B.A., Luzardo, G., Goldin, S.B., and Rosemurgy, A.S. (2006). Prognostic significance of new onset ascites in patients with pancreatic cancer. World J. Surg. Oncol. *4*, 16.

Zheng, G.X., Terry, J.M., Belgrader, P., Ryvkin, P., Bent, Z.W., Wilson, R., Ziraldo, S.B., Wheeler, T.D., Mcdermott, G.P., Zhu, J., et al. (2017). Massively parallel digital transcriptional profiling of single cells. Nat. Commun. *8*, 14049.

Zhu, Y., Herndon, J.M., Sojka, D.K., Kim, K.W., Knolhoff, B.L., Zuo, C., Cullinan, D.R., Luo, J., Bearden, A.R., Lavine, K.J., et al. (2017). Tissue-resident macrophages in pancreatic ductal adenocarcinoma originate from embryonic hematopoiesis and promote tumor progression. Immunity *47*, 323–338.e6.

Please cite this article in press as: Alam et al., Fungal mycobiome drives IL-33 secretion and type 2 immunity in pancreatic cancer, Cancer Cell (2022), https://doi.org/10.1016/j.ccell.2022.01.003

STAR★METHODS

KEY RESOURCES TABLE

REAGENT or RESOURCE	SOURCE	IDENTIFIER
Antibodies		
mIL-33	R&D	Cat# AF3626; RRID: AB_884269
hIL-33	R&D	Cat# AF3625; RRID: AB_1151900
beta-actin	Sigma	Cat# A2228; RRID: AB_476697
CD4	Abcam	Cat# ab133616; RRID: AB_2750883
CD45	Abcam	Cat#ab10558; RRID: AB_442810
p-STAT6	Cell signaling technology	Cat# 56554S; RRID: AB_2799514
pAKT-S473	Cell signaling technology	Cat# 9271S; RRID: AB_329825
pERK-p44/42	Cell signaling technology	Cat# 4370S; RRID: AB_2315112
pan-keratin	Cell signaling technology	Cat# 4545S; RRID: AB_490860
CARD9	Cell signaling technology	Cat# 12283S; RRID AB_2797869
Src	Cell signaling technology	Cat# 2108s; RRID: AB_331137
Phospho-Syk (Tyr525/526)	Cell signaling technology	Cat# 2710s; RRID: AB_2197222
Phospho-Src Family (Tyr416)	Cell signaling technology	Cat# 6943s; RRID: AB_10013641
Syk	Cell signaling technology	Cat# 2712s; RRID: AB_2197223
Phospho-NF-κB p65 (Ser536)	Cell signaling technology	Cat# 13346T; RRID: AB_2798185
Phospho-IRF-3 (Ser396)	Cell signaling technology	Cat# 29047T; RRID: AB_2773013
Phospho-IRF-7 (Ser477)	Cell signaling technology	Cat# 12390T; RRID: AB_2797896
Anti-rabbit IgG, HRP-linked	Cell signaling technology	Cat# 7074P2; RRID: AB_2099233
Mouse on mouse horseradish peroxidase polymer	Biocare medical	Cat# MM510
Rabbit on rodent horseradish peroxidase polymer	Biocare medical	Cat# RMR622
Goat on rodent horseradish peroxidase polymer	Biocare medical	Cat# GHP516
Goat probe	Biocare medical	Cat# GP626L
Donkey anti Goat IgG Alexa Flour Plus 488	Invitrogen	Cat# A32814; RRID: AB_2762838
Donkey anti Rabbit Alexa Flour Plus 555	Invitrogen	Cat# A32794; RRID: AB_2762834

(*Continued on next page*)

Please cite this article in press as: Alam et al., Fungal mycobiome drives IL-33 secretion and type 2 immunity in pancreatic cancer, Cancer Cell (2022), https://doi.org/10.1016/j.ccell.2022.01.003

Continued

REAGENT or RESOURCE	SOURCE	IDENTIFIER
A32814 secondary antibody IgG goat	Biorad	Cat# 1721034; RRID: AB_11125144
A32794 secondary antibody anti IgG rabbit	Biorad	Cat# 1706515; RRID: AB_11125142
Zombi UV	Biolegend	Cat# 423107
BV421 Lin$^-$	Biolegend	Cat# 133311; RRID: AB_11203535
BV510 B220	Biolegend	Cat# 103247; RRID: AB_2561394
BV605 CD11b	Biolegend	Cat# 101237; RRID: AB_11126744
BV605 KLRG1	Biolegend	Cat# 138419; RRID: AB_2563357
BV785 ICOS	Biolegend	Cat# 313533; RRID: AB_2629728
FITC GR1	Biolegend	Cat# 108405; RRID: AB_313370
FITC CD90.2	Biolegend	Cat# 140303; RRID: AB_10642686
PerCP CD25	Biolegend	Cat# 102027; RRID: AB_893290
PE CD11c	Biolegend	Cat# 117307; RRID: AB_313776
PE CCR4	Biolegend	Cat# 131203; RRID: AB_1236369
PE F4/80	Biolegend	Cat# 123109; RRID: AB_893498
PE-Cy5 CD127	Biolegend	Cat# 135015; RRID: AB_1937262
PE Cy7 Ly6G	Biolegend	Cat# 127617; RRID: AB_1877262
PE Cy7 CD4	Biolegend	Cat# 100421; RRID: AB_312706
PE Cy7 ST2	Biolegend	Cat# 146609; RRID: AB_2728178
APC Ly6C	Biolegend	Cat# 128015; RRID: AB_1732087
APC CD3	Biolegend	Cat# 100235; RRID: AB_2561455
APC Sca1	Biolegend	Cat# 108111; RRID: AB_313348
AF647 eFlour 640 MHC II	Biolegend	Cat# 107617; RRID: AB_493526
AF700 CD11b	Biolegend	Cat# 101220; RRID: AB_493546
APC-Cy7 CD45	Biolegend	Cat# 103115; RRID: AB_312980
Brilliant Violet 421 Rat IgG2b	Biolegend	Cat# 400639; RRID: AB_10895758
Ultra-LEAF Purified Rat IgG2b	Biolegend	Cat# 400644; RRID: AB_11149687
PE/Cy7 Rat IgG1	Biolegend	Cat# 400416; RRID: AB_326522

(*Continued on next page*)

Please cite this article in press as: Alam et al., Fungal mycobiome drives IL-33 secretion and type 2 immunity in pancreatic cancer, Cancer Cell (2022), https://doi.org/10.1016/j.ccell.2022.01.003

Continued

REAGENT or RESOURCE	SOURCE	IDENTIFIER
APC Rat IgG2a	Biolegend	Cat# 400512; RRID: AB_2814702
PE/Cyanine5 Rat IgG2a	Biolegend	Cat# 400510
PerCP/Cyanine5.5 Mouse IgG2b	Biolegend	Cat# 400338
Brilliant Violet 421 FOXP3	Biolegend	Cat# 126419; RRID: AB_2565933
Brilliant Violet 785 CD8a	Biolegend	Cat# 100749; RRID: AB_2562610
Brilliant Violet 421(TM) anti-human FOXP3	Biolegend	Cat# 320124; RRID: AB_2565972
APC/Cyanine7 anti-human CD45	Biolegend	Cat# 304014; RRID: AB_314402
APC anti-human CD3	Biolegend	Cat# 317318; RRID: AB_1937212
PE/Cyanine7 anti-human CD4	Biolegend	Cat# 317414; RRID: AB_571959
Brilliant Violet 785(TM) anti-human CD8	Biolegend	Cat# 344740; RRID: AB_2566202
PE anti-mouse/human KLRG1 (MAFA)	Biolegend	Cat# 138408; RRID: AB_10574313
APC anti-human Lineage Cocktail (CD3, CD14, CD16, CD19, CD20, CD56)	Biolegend	Cat# 348803
PE/Cyanine5 anti-human CD127 (IL-7Ralpha)	Biolegend	Cat# 351324; RRID: AB_10915554
FITC anti-human CD25	Biolegend	Cat# 302604; RRID: AB_314273
Human TruStain FcX™	Biolegend	Cat# 422302; RRID: AB_2818986
Alexa Fluor(R) 488 anti-human FOXP3	Biolegend	Cat# 320112; RRID: AB_430883
PerCP/Cyanine5.5 anti-GATA3	Biolegend	Cat# 653812; RRID: AB_2563219
Mouse Anti-Human CD4	Becton Dickinson	Cat# 560345; RRID: AB_1645572
CD3	Becton Dickinson	Cat# 560176; RRID: AB_1645475
CD8	Becton Dickinson	Cat# 560347; RRID: AB_1645581
CD127 (IL-7 Receptor a subunit)	Becton Dickinson	Cat# 557938; RRID: AB_2296056
Human ST2/IL-33R APC	R&D	Cat# FAB5231A
Brilliant Violet 510™ anti-human Lineage Cocktail (CD3, CD14, CD16, CD19, CD20, CD56)	Biolegend	Cat# 348807
PE anti-human CD25	Biolegend	Cat# 302606; RRID: AB_314276
Bacterial and virus strains		
Alternaria alternata	ATCC	Cat# ATCC 36376
Malassezia globosa	ATCC	Cat# MYA-4889
Alternaria alternata extract	Stallergenes Greer Lab	Cat# XPM1D3a.5
Candida albicans extract	Stallergenes Greer Lab	Cat# XPLM73X1A2

(*Continued on next page*)

Please cite this article in press as: Alam et al., Fungal mycobiome drives IL-33 secretion and type 2 immunity in pancreatic cancer, Cancer Cell (2022), https://doi.org/10.1016/j.ccell.2022.01.003

Continued

REAGENT or RESOURCE	SOURCE	IDENTIFIER
Aspergilus fumigatus extract	Stallergenes Greer Lab	Cat# XPM3D3A4
Biological samples		
Human fresh PDAC samples	Roswell Park Cancer Center	Project approval number MOD00008843/ BDR 135920
Human PDAC TMA	MD Anderson Cancer Center	Project approval number LAB05-0854
Chemicals, peptides, and recombinant proteins		
DiD solid	Fisher	Cat# D7757
PD184352 (CI-1040)	Selleck Chem	Cat# S1020
Trametinib (GSK1120212)	Selleck Chem	Cat# S2673
ECL select western blot detection	Fisher	Cat# 45-000-999
Chitinase from *S. griseus*	Sigma-Aldrich	Cat# 2593-74-2
xylenes	Fisher	Cat# 1330-20-7
hematoxylin	Fisher	Cat# 517-28-2
tween 20	Biorad	Cat# 9005-64-5
trizol	Sigma-Aldrich	Cat# 136426-54-5
chloroform	Sigma-Aldrich	Cat# 67-66-3
proteinase K	Thermo Fisher Scientific	Cat# EO0491
blotting grade buffer	Biorad	Cat# 999999-99-4
20X MOPS buffer	Fisher	Cat# 1132-61-2
sodium n-dodecyl sulfate	Fisher	Cat# 151-21-3
Triton-x 100	Fisher	Cat# 9002-93-1
Tween 40	Fisher	Cat# 9005-66-7
ox-bile	Sigma-Aldrich	Cat# 8008-63-7
peptone	Sigma-Aldrich	Cat# 91079-38-8
tris buffered saline tween 20 (TBST)	Corning	Cat# 7732-18-5
western blot stripping buffer	Fisher	Cat# 21059
formaldehyde solution	Fisher	Cat# 50-00-0
10% neutral buffered formalin	Fisher	Cat# 7558-80-7
glucose solution	Corning	Cat# 50-99-7
penicillin-streptomycin 100x	Corning	Cat# 63936-85-6
glutamax 100x	Corning	Cat# 333-93-7
bambanker freezing media	Corning	Cat# NC9582225
MEM non essential amino acids (NEAA)	Corning	Cat# 70-47-3
sodium pyruvate	Corning	Cat# 113-24-6
fetal bovine syrum (FBS)	Fisher	Cat# 9014-81-7
0.25% trypsin	Corning	Cat# 2594-14-1
l-glutamate 100x	Corning	Cat# 56-86-0
collagenase IV	stem cell technologies	Cat# 07909
dispase	stem cell technologies	Cat# 07923
ficoll-paque plus	Fisher	Cat# 17-1440-02
amphotericin b	Fisher	Cat# 1397-89-3
doxycycline	Sigma-Aldrich	Cat# 564-25-0
DNase I	Fisher	Cat# 9003-98-9
puromycin	Fisher	Cat# 58-58-2
buparlisib (BKM120)	Selleck Chem	Cat# 944396-07-0
RPMI	Corning	Cat# 10-040-CV
DMEM	Corning	Cat# 10-017-CV
IL-7	R&D	Cat# 407-ML-005
IL-33	Peprotech	Cat# 210-33
IL-2	Peprotech	Cat# 212-12

(*Continued on next page*)

Please cite this article in press as: Alam et al., Fungal mycobiome drives IL-33 secretion and type 2 immunity in pancreatic cancer, Cancer Cell (2022), https://doi.org/10.1016/j.ccell.2022.01.003

Continued

REAGENT or RESOURCE	SOURCE	IDENTIFIER
Qiazol	Qiagen	Cat# 79306
Critical commercial assays		
LEGEND MAX™ Mouse IL-33 ELISA Kit	Biolegend	Cat# 436407
Mouse IL-5 Quantikine ELISA Kit	R&D	Cat# M5000
Mouse IL-13 Culture Media Quantikine ELISA	R&D	Cat# M1300CB
Cell fractionation kit	Abcam	Cat# ab109719
Lipofectamine 3000	Invitrogen	Cat# L3000015
NextSeq 500 High Output Kit	Illumina	Cat# 20024906
Mouse Tumor Dissociation kit	Miltenyi Biotec	Cat# 130-096-730
Qubit Broad Range DNA kit	Thermofisher	Cat# Q32853
MycoAlert Mycoplasma Detection Kit	Lonza	Cat# LT07-218
DNeasy Powersoil Pro Kit	Qiagen	Cat# 47014
DC Protein Assay Kit	Biorad	Cat# 5000111
Nextera Index Kit	Illumina	Cat# FC-131-1024
iTaq Universal SYBR Green Supermix	BioRad	Cat# 1725121
iScript™ cDNA Synthesis Kit	Biorad	Cat# 1708891
EasySep™ Mouse ILC2 Enrichment Kit	Stem Cell Technologies	Cat# 19842
Cas9 Protein	Sigma-Aldrich	Cat# CAS9PROT-50UG
Deposited data		
UNITE's Fungi taxon (v8.4)	https://unite.ut.ee/repository.php	N/A
The Human Protein Atlas	https://www.proteinatlas.org/	N/A
Oncomine	https://www.oncomine.org/resource/login.html	N/A
RNAseq of mouse PDAC cell lines	This paper	GEO: GSE190468
scRNAseq of CD45 cells	This paper	GEO: GSE190103
18s rRNA sequencing	This paper	BioSample accessions: SAMN23523449, SAMN23523450, SAMN23523451, SAMN23523452, SAMN23523453, SAMN23523454, SAMN23523455, SAMN23523456
Experimental models: Cell lines		
AK-B6	From Ron DePinho	PMID: 32046984
KPC1199	From Michael Feigin	N/A
PJ-B6-4298	This study	N/A
PJ-B6-4291	This study	N/A
PJ-B6-4271	This study	N/A
AK138	From Ron DePinho	PMID: 32046984
AK192	From Ron DePinho	PMID: 32046984
HY15549	From Ron DePinho	PMID: 32046984
HY19636	From Ron DePinho	PMID: 32046984
AK14838	From Ron DePinho	PMID: 32046984
HEK 293T	ATCC	CRL-3216
Experimental models: Organisms/strains		
Mouse:C57BL/6J	The Jackson Laboratory	Cat# 000644 IMSR_JAX:006362
Mouse:B6.129S4-Krastm4Tyj/J	The Jackson Laboratory	Cat# 008179 IMSR_JAX:008179
Mouse:B6.FVB-Tg(Pdx1-cre)6Tuv/J	The Jackson Laboratory	Cat# 014647 IMSR_JAX:014647

(*Continued on next page*)

Please cite this article in press as: Alam et al., Fungal mycobiome drives IL-33 secretion and type 2 immunity in pancreatic cancer, Cancer Cell (2022), https://doi.org/10.1016/j.ccell.2022.01.003

Continued

REAGENT or RESOURCE	SOURCE	IDENTIFIER
Mouse:B6.129P2-Trp53tm1Brn/J	The Jackson Laboratory	Cat# 008462 IMSR_JAX:008462
Mouse:TetO_Lox-Stop-Lox-Kras^{G12D} (tetO_Kras^{G12D})	From Ron DePinho	PMID: 22541435
Mouse:ROSA26-LSL-rtTA-IRES-GFP (ROSA_rtTA)	From Ron DePinho	PMID: 22541435
129S-Trp53tm2Tyj/J	The Jackson Laboratory	Cat# 008652 IMSR_JAX:008652
Mouse:p48-Cre	From Ron DePinho	PubMed:17301087
Oligonucleotides		
See Table S1	N/A	N/A
Recombinant DNA		
pLKO.1	Addgene	Cat# 10878 **A lentiviral RNAi library for human and mouse genes applied to an arrayed viral high-content screen.** Moffat J, Grueneberg DA, Yang X, Kim SY, Kloepfer AM, Hinkle G, Piqani B, Eisenhaure TM, Luo B, Grenier JK, Carpenter AE, Foo SY, Stewart SA, Stockwell BR, Hacohen N, Hahn WC, Lander ES, Sabatini DM, Root DE *Cell*. *2006 Mar 24*. *124*(6):*1283-98*.
psPAX2	Addgene	Cat# 12260 psPAX2 was a gift from Didier Trono (Addgene plasmid # 12260; http://n2t.net/addgene:12260; RRID:Addgene_12260)
pMD2.G	Addgene	Cat# 12259 pMD2.G was a gift from Didier Trono (Addgene plasmid # 12259; http://n2t.net/addgene:12259; RRID:Addgene_12259)
Software and algorithms		
FlowJo	FlowJo, LLC	N/A
GraphPad Prism 8.4.3	GraphPad Software	N/A
Biorad CFX Manager	BioRad	Cat# 184500
Leica DM3000 LED	Leica Microsystems	Cat# 11888844
Stelaris 5 Confocal Microscope	Leica Microsystems	N/A
Li-Cor Odyssey Fc	Li-Cor Biosciences	Cat# 2800
CFX Connect Real-Time PCR Detection System	BioRad	Cat# 1855201
IVIS Spectrum Imaging System	Perkin Elmer	N/A
ParaVision 3.0.2	Paravision	N/A
Living Image 4.7	Perkin Elmer	N/A
Illumina HiSeq2000	Illumina	N/A
Agilent 2200 Tapestation	Agilent	N/A
BD LSR	Becton Dickinson	N/A
Aperio ScanScope XT	Aperio	N/A
Aperio ImageScope	Aperio	N/A
Olympus BX61	Olympus	N/A
Tapestation 4200 D1000	Agilent	N/A
MiSeq	Illumina	N/A
R Studio	R Studio	N/A

Please cite this article in press as: Alam et al., Fungal mycobiome drives IL-33 secretion and type 2 immunity in pancreatic cancer, Cancer Cell (2022), https://doi.org/10.1016/j.ccell.2022.01.003

RESOURCE AVAILABILITY

Lead contact

Further information and requests for resources and reagents should be directed to and will be fulfilled by the lead contact, Prasenjit Dey (prasenjit.dey@roswellpark.org).

Materials availability

Upon request mouse cell lines (PJ-B6-4291, PJ-B6-4298 and PJ-B6-4271) generated in the lab will be made available.

Data and code availability

Processed single-cell RNA-seq and RNA-seq data of this study can be obtained from Gene Expression Omnibus (GEO) with an accession number of GSE190103 and GSE190468, respectively. 18s rRNA seq data can be obtained from BioSample accessions: SAMN23523449, SAMN23523450, SAMN23523451, SAMN23523452, SAMN23523453, SAMN23523454, SAMN23523455, SAMN23523456.

All other data are available from the corresponding authors upon request.

EXPERIMENTAL MODEL AND SUBJECT DETAILS

Ethics statement and animal modeling

All animal procedures were approved by Institutional Animal Care and Use Committee (IACUC) at Roswell Park Comprehensive Cancer Center. All animals were maintained in pathogen-free conditions and cared for in accordance with the International Association for Assessment and Accreditation of Laboratory Animal Care policies and certification. All surgeries were performed with isoflurane anesthesia. Analgesic (Buprenorphine) was administered after surgery along with temperature-controlled post-surgical monitoring to minimize suffering. TetO_Lox-Stop-Lox-Kras^{G12D} (tetO_Kras^{G12D}), ROSA26-LSL-rtTA-IRES-GFP (R26_rtTA), Ptf1a-Cre, LSL-Trp53, LSL-Kras^{G12D}, LSL-Trp53^{R172H} and Pdx1-Cre strains were described previously (Ying et al., 2012; Olive et al., 2004; Hingorani et al., 2003). Mice were backcrossed to the C57BL/6 background for more than 8 generations to achieve a pure B6 mouse, and the purity and zygosity of iKPC mouse was validated by Charles River. Mice with spontaneous pancreatic tumors were euthanized at designated time points for tumor collection. Owing to the internal location of these tumors, we used signs of lethargy, reduced mobility, and morbidity, rather than maximal tumor size, as a protocol-enforced endpoint.

Human PDAC primary tumor samples

Fresh human PDAC samples were obtained from Roswell Park Comprehensive Cancer Center's tissue Biobank. Human studies were approved by Roswell Park Comprehensive Cancer Center's Institutional Review Board, and prior informed consent was obtained from all subjects and the tissues were distributed under IRB protocol STUDY00001407/BDR 135920. Fresh human PDAC samples were processed to obtain single cell suspension using a tissue dissociation cocktail consisting of Collagenase IV (Cat. No.: 07909, Stem Cell Technologies), Dispase (Cat. No.: 07923, Stem Cell Technologies) and DNase I (Cat. No.: 9003-98-9, Fisher Scientific) in a DMEM/F12 with 15 mM HEPES media. For flow cytometry analysis samples were further processed as described below in the section "flow cytometry". Fluorochrome-conjugated antibodies against CD45 (304014), Foxp3 (320124 and 320112), CD3 (317318), CD4 (317414), CD8 (344740), KLRG1 (138408), Lin$^-$ cocktail (348803), CD127 (351324), CD25 (302604), TruStain FcX (422302), Gata-3 (653812) were purchased from Biolegend and ST2 (FAB5231A) from R&D. To assess cell viability, cells were incubated with Zombie UV (423107, Biolegend), prior to FACS analysis. All samples were acquired with the BD LSR analyzer (Becton Dickinson) and analyzed with FlowJo software (Tree Star).

Human PDAC TMA samples were obtained from MD Anderson Cancer Center Biobank. Human studies were approved by MD Anderson's Institutional Review Board (IRB), and prior informed consent was obtained from all subjects under IRB protocol LAB05-0854. The samples were stained using the standard IHC protocol. The antibodies used were IL-33 (R&D systems, AF3626) and secondary antibody (HRP-polymers, Biocare Medical). The stained samples were imaged using Aperio ScanScope XT scanner and Aperio ImageScope software was used for image visualization and analysis. Staining intensity of tissue sections was scored in a 'blinded' manner by a pathologist.

Mice and tumor models

For all experiments, C57BL/6J (Stock 000664) mice, aged 4–6 weeks were obtained from Jackson Laboratory unless otherwise mentioned. For orthotopic pancreas transplantation, mice were anesthetized using isoflurane. A 2x2-mm portion of the left abdomen was shaved to facilitate transplantation. An incision was made in the left abdomen and the pancreas was gently exposed along with the spleen. Luciferase-expressing cells (AK-B6-RFP-Luc) were slowly injected into the tail of the pancreas using a Hamilton syringe. Twenty microliters of cells (5×10^5) mixed with 20 μL of Matrigel were injected. For the orthotopic model, animals were imaged (IVIS Spectrum, PerkinElmer) 2 days after surgery to assess successful implantation of the tumors. Only orthotopic tumors of similar luciferase intensity were used further for the study. For iKPC cell line, chow supplemented with Dox was started after transplantation. Furthermore, in early stages the progress of the tumor is monitored by MRI and/or IVIS Spectrum imaging and in the late stages of the tumor development by MRI alone. The upper limit for the tumor volume is set at 4,000 mm^3. However, owing to the internal

Please cite this article in press as: Alam et al., Fungal mycobiome drives IL-33 secretion and type 2 immunity in pancreatic cancer, Cancer Cell (2022), https://doi.org/10.1016/j.ccell.2022.01.003

location of the tumors, we used signs of lethargy, reduced mobility, and morbidity, rather than maximal tumor size, as a protocol-enforced endpoint. Typically, mice are sacrificed around day 28 or if moribund because of tumor burden, which is considered as an endpoint.

METHOD DETAILS

In vivo imaging

In vivo live imaging was performed at the Animal Imaging Facility at Roswell Park Comprehensive Cancer Center. Magnetic resonance imaging (MRI) was performed using a 4.7 Tesla, preclinical scanner using the ParaVision 3.0.2 platform and a 35 mm I.D. radio-frequency coil (Bruker Biospin, Billerica, MA). Mice were anesthetized with isoflurane. Temperature and respiration were regulated using an MR-compatible small animal monitoring system (Model 1250, SAII, Stony Brook, NY.) Following scout scans, tumor burden was determined using multislice, fast spin echo scans in the axial and coronal planes. Both sets of images used a TE/TR = 40/2,500 ms, an echo train length = 8, slice thickness = 1 mm, acquisition matrix = 256 × 192 and 4 averages/NEX. Coronal images were acquired with a field of view (FOV) = 48 × 32 mm, while axial images were acquired with a FOV = 32 × 32 mm. A subset of axial scans required a larger number of slices to capture tumor growth, which increased the repetition time to 3,600 ms. Tumor volumes were calculated by manual segmentation and voxel summation using commercially available, medical image processing software (Analyze 10.0, AnalyzeDirect, Overland Park, KS).

For bioluminescent imaging, animals were anesthetized with isoflurane, injected intraperitoneally with 3 mg of D-Luciferin (Perkin Elmer) and imaged using IVIS Spectrum Imaging System (Perkin Elmer). The Living Image 4.7 software (Perkin Elmer) was used for analysis of the images post acquisition.

Transcriptomic profiling by RNA-seq and qRT-PCR

For RNAseq, total RNA was isolated using QIAzol extraction (Cat. No.: 79306, Qiagen) followed by purification with the Qiagen RNAeasy kit as described previously (Dey et al., 2012). Libraries were generated using Illumina's TruSeq RNA Library Prep Kit v2 and were sequenced using the Illumina HiSeq 2000 Sequencer with 76 nt single-end read. Raw read RNA-seq data were mapped to GRCm38-mm10 reference genome using STAR aligner (Dobin et al., 2013). HTSEQ-COUNT (Anders et al., 2015) was used to count raw reads in each gene for each sample. Differential expression analysis was performed with edgeR (Robinson et al., 2010) and pathway enrichment analysis was performed with GSEA software. For qRT-PCR, RNA samples were reverse transcribed into cDNA using the High-Capacity cDNA Reverse Transcript kit (Life Technologies). cDNA samples were subjected to qRT-PCR quantification in duplicates using iTaq Universal SYBR Green Supermix (BioRad) according to the product guides on BioRad CFX96 Real Time machine. The primer sequences used for qRT-PCR are the following: *Il33* (Fwd 5′-TGAGACTCCGTTCTGGCCTC-3′, Rev 5′-CTCTTCATGCTTGGTACCCGAT-3′), *Actb* (Fwd 5′-GGCTGTATTCCCCTCCATCG-3′, Rev 5′-CCAGTTGGTAACAATGCCATGT-3′), *Tph1* (Fwd 5′-CACGAGTGCAAGCCAAGGTTT-3′, Rev 5′-AGTTTCCAGCCCCGACATCAG-3′), *Il13* (Fwd 5′-TGAGGAGCTGAGCAACATCACACA-3′, Rev 5′-TGCGGTTACAGAGGCCATGCAATA-3′), *Il5* (Fwd 5′-TCACCGAGCTCTGTTGACAA-3′, Rev 5′-CCACACTTCTCTTTTTGGCG-3′), and Amphiregulin (*Areg*) (Fwd 5′-GGTCTTAGGCTCAGGACATTA-3′, Rev 5′-CGCTTATGGAAACCTCTC-3′) (Table S1).

Single cell RNA sequencing (scRNAseq)

For scRNAseq, live CD45$^+$ cells were flow sorted by BD FACSAria. Single cell libraries were generated using the 10X Genomics Chromium Single Cell 3′ GEM, Library & Gel Bead Kit v3, (10x Genomics, Cat.: 1000075). Briefly, single cell suspensions were first assessed with Trypan Blue using Thermo Fisher Countess II FL Automated Cell Counter (ThermoFisher), to determine concentration, viability and the absence of clumps and debris that could interfere with single cell capture. The cells were then loaded into the Chromium Controller (10x Genomics) where they are partitioned into nanoliter-scale Gel Beads-in-emulsion. Reverse transcription was performed, and the resulting cDNA was amplified following the manufacturer's instructions. The full-length amplified cDNA was used to generate gene expression libraries by enzymatic fragmentation, end-repair, a-tailing, adapter ligation, and PCR to add Illumina compatible sequencing adapters. The resulting libraries were evaluated on D1000 screentape using a TapeStation 4200 (Agilent Technologies) and quantitated using Kapa Biosystems qPCR quantitation kit for Illumina. Final libraries were then pooled, denatured, and diluted to 300 p.m. with 1% PhiX control library added. The resulting pool was then loaded into the Illumina NovaSeq Reagent cartridge and sequenced on a NovaSeq 6000 following the manufacturer's recommended protocol (Illumina Inc.).

scRNAseq data analysis

FASTQ files were processed using 10x Genomics Cell Ranger 6.0.0 pipeline to align reads and generate feature-barcode matrices. The Cell Ranger output was further used for detailed data analysis. For the Chromium 10x Genomics libraries, the raw sequencing data were processed using Cell Ranger software to generate the fastq files and count matrices (Zheng et al., 2017). Then the filtered gene-barcode matrices which contain barcodes with the Unique Molecular Identifier (UMI) counts that passed the cell detection algorithm was used for further analysis. The downstream analyses were performed primarily using Seurat single cell data analysis R package (Hao et al., 2021). First, cells with unique feature counts over 5,000 or less than 200, or cells that have >20% mitochondrial counts were filtered out from the analysis to remove dead cells. Additionally, a cell cycle score for S and G2/M phases based on the well-defined gene sets was assigned to each cell using CellCycleScoring function from Seurat. Then the normalized and scaled UMI counts were calculated using the SCTransform method and be regressed against the cell cycle scores. Dimension reductions

including principal component analysis (PCA), UMAP and tSNE were performed for the highly variable genes. Data clustering were identified using the shared nearest neighbor (SNN)-based clustering on the first 30 principal components. SingleR package was utilized to identify the immune cell types using ImmGen reference dataset (Aran et al., 2019).

Flow cytometry

Single cells from tumor were isolated using the Mouse Tumor Dissociation kit (Cat.: 130-096-730, Miltenyi Biotec) based on manufacturer's protocol. Cells from spleen were isolated by mincing with a 5-mL syringe plunger against a 70 μm cell strainer into a 50 mL falcon tube using Roswell Park Memorial Institute (RPMI) medium. The cells were depleted of erythrocytes by RBC lysis buffer (Biolegend, Cat.: 420302). Peripheral blood (100 μL) was drawn using retroorbital bleeding and depleted of erythrocytes by RBC lysis buffer. Next, tumor, spleen or blood cells were incubated with CD16/CD32 antibody (clone 2.4G2, BD Biosciences) to block FcγR binding for 10 min then with a antibody mix for 30 min at room temperature. Fluorochrome-conjugated antibodies against CD45 (103115), CD11b (101220), CD11b (101237), Gr-1 (108405), Ly-6C (128015), Lineage cocktail (133311), B220 (103247), Ki67 (350521), KLRG1 (138419), ICOS (313533), GR1 (108405), CD45RB (151607), EpCAM (118207), CD62L (104405), CCR3 (144509), CD90.2 (140303), CD25 (102027), CD11c (117307), CD44 (103023), CCR4 (131203), CD117 (105807), F4/80 (123109), CD86 (105016), CD127 (135015), ST2 (146609), Ly-6c (128015), CD3 (100235), Sca1(108111), Gata3 (653812), Ly-6G (127617), CD4 (100421), CD3 (100235), CD8 (100749) were purchased from BioLegend. To assess cell viability, cells were incubated with Zombie UV (423107, Biolegend), prior to FACS analysis. All samples were acquired with the BD LSR analyzer (Becton Dickinson) and analyzed with FlowJo software (Tree Star).

Immunoblotting and antibodies

Cell culture medium were removed, and the cells were washed twice in ice-cold phosphate-buffered saline (PBS). Cells are scraped and transferred to an Eppendorf tube, followed by centrifugation at 1, 700 *g* for 5 min. The pelleted cells were incubated in radio immune precipitation assay (RIPA) buffer with proteinase and phosphatase inhibitors for 15 min. Lysates were then collected and centrifuged at 12,000 rpm for 15 min at 4°C. Protein concentration was measured using the DC Protein Assay Kit (Biorad, 5000111). SDS–PAGE and immunoblotting were performed as described previously in a pre-cast bis-Tris 4–20% gradient gels (Invitrogen) (Dey et al., 2017). The following antibodies were used: The following antibodies were used: IL-33 (R&D systems, AF3626); pAKT-S473 (CST, 9271); pERK1/2 (CST, 4370); CARD9 (CST, 2283s); Src (CST, 2108s); Phospho-Syk-Y525/526 (CST, 2710s); Phospho-Src-Y416 (CST, 6943s); Syk (CST, 2712s) and β-Actin (Sigma-Aldrich, A2228).

Immunohistochemistry and immunofluorescence

Harvested tissues were immediately fixed in 10% formalin overnight followed by incubation in 70% ethanol for 48 h. Fixed tissues are then processed in tissue processor and embedded in paraffin. IHC was performed as described previously (Dey et al., 2014). Briefly, endogenous peroxidases were inactivated by 3% hydrogen peroxide. Non-specific signal was blocked using 5% BSA for 30 min in 0.1% Tween 20. Tumor samples were stained with the following primary antibodies: CD45 (Abcam, ab10558), mouse IL-33 antibody (R&D systems, AF3626); human IL-33 antibody (R&D systems, AF3625); SMA (abcam, ab5694) and Pan-Keratin (CST, 4545S). After overnight incubation, the slides were washed and incubated with secondary antibody (HRP-polymers, Biocare Medical) for 30 min at room temperature. The slides were washed three times and stained with DAB substrate (ThermoFisher Scientific). The slides were then counterstained with haematoxylin and mounted with mounting medium. For immunofluorescence tissues were stained with primary antibodies overnight followed by staining with fluorescence labeled secondary antibodies at room temperature for 2 h. The nuclei is stained with DAPI. Immunofluorescence slides were imaged with Leica confocal Microscope and quantified with ImageJ.

Cell culture and establishment of primary PDAC lines

Following primary mouse cell lines were established in the laboratory (PJ-B6-4291, PJ-B6-4298 and PJ-B6-4271). The following cell lines are a gift from Dr. Ronald De-Pinho (AK-B6, AK14838, AK192, HY19636, HY15559) as described previously (Aguirre et al., 2003) and Dr. Michael Feigin (KPC1199). All cell lines were routinely cultured in RPMI 1640 (Invitrogen) in 10% FBS (Invitrogen), 100 U/mL penicillin and 100 U/mL streptomycin. For inducible KPC derived cell lines, 1 μg/mL of doxycycline was directly added to the media. The cell lines were mycoplasma free, based on tests done monthly in the laboratory using Lonza's MycoAlert Mycoplasma Detection Kit assays with confirmatory tests by PCR-based assays.

shRNA and CRISPR-Cas9 knockdown

shRNA knockdown was performed as described previously (Dey et al., 2017). We screened 3-5 hairpins targeting the gene of interest and found two independent sequences that reduced mRNA levels by >60%. The shRNA sequences were as follows: *Il-33* 5′-CCGG GCATCCAAGGAACTTCACTTTCTCGAGAAAGTGAAGTTCCTTGGATGCTTTTTTG-3′ (TRCN0000173352) and 5′-CCGGCCATAA GAAAGGAGACTAGTTCTCGAGAACTAGTCTCCTTTCTTATGGTTTTTTG-3′ (TRCN0000176387); 3′ (Table S1). A non-targeting shRNA (shCtrl) was used as a control. The shRNA-expressing pLKO.1 vector was introduced into cancer cell lines by lentiviral infection. Recombinant lentiviral particles were produced by transient transfection of 293T cells following a standard protocol. Briefly, 10 μg of the shRNA plasmid, 5 μg of psPAX2 and 2.5 μg of pMD2.G were transfected using Lipofectamine 3000 (Invitrogen) into 293T cells plated in a 100-mm dish. Viral supernatant was collected 72 h after transfection, centrifuged to remove any 293T cells and filtered (0.45 μm). For transduction, viral solutions were added to cell culture medium containing 4 μg/mL polybrene; 48 h after infection, cells were selected

Please cite this article in press as: Alam et al., Fungal mycobiome drives IL-33 secretion and type 2 immunity in pancreatic cancer, Cancer Cell (2022), https://doi.org/10.1016/j.ccell.2022.01.003

using 2 μg/mL puromycin and tested for gene depletion by qRT–PCR or immunoblotting. For CRISPR-Cas9 knockdown of *Il33*, sgRNAs were purchased from Synthego (Sanger CRISPR clones). The sgRNAs along with Cas9 protein (sigma) was transfected into PDAC cells and single cell clones were FACS sorted. The sgIL33 sequence used for *Il33* DNA sequence targeting. 5′-AUAGUAGCGUAGCGUAGUAGCACC-3′ and 5′-AUCUCUUCCUAGAAUCCCG-3′ (Table S1). The clones were validated by western blot for deletion of IL-33.

Anti-fungal treatment and fungal challenge experiments

For anti-fungal treatment experiments, PDAC cell lines were treated with 0.1 μg/ul (final concentration) of fungal extract (*A. alternata*, XPM1D3a.5, *Candida albicans*, XPLM73 X1A2 and *Aspergilus fumigatus*, XPM3D3A4, Stallergenes Greer Lab) for different time points (2, 3, 6 and 24 h). The fungal extract treated spent media from PDAC cell culture was used for IL-33 cytokine profiling by ELISA. The fungal extract treated PDAC cell extract was used for western blotting. All the experiments were performed in a biosafety cabinet following Roswell Park Cancer Center bio-safety guidelines. For gastrointestinal fungal depletion, C57BL/6 mice were treated with 200 μg amphotericin B per day by oral gavage for five consecutive days, followed by 0.5 μg/mL amphotericin B treatment in drinking water for 21 days. Control groups were gavage with 200 μL of PBS for 5 consecutive days. After completion of anti-fungal treatment, species specific fungal repopulation was done with *A. alternata* (ATCC, 36376) and *M. globosa* (MYA-4889). Fungi were administered (1×10^8 CFU/mL) by oral gavage. Seven days after fungal administration, PDAC cells were orthotopically transplanted.

Fungal fluorescence in situ hybridization (FISH)

FISH was done on a 4 μm thick paraffin embedded pancreatic tissue sections. Sections were pretreated using a commercially available kit (Cytocell, Inc) according to manufacturer's instructions. For Hybridization, D223 28S rRNA gene probe (Molecular probe, Thermo Fisher Scientific) (Table S1) labeled with the 6-FAM fluorophore (extinction wavelength, 488 nm; emission wavelength, 530 nm) was used to detect the fungal colonization within the mouse pancreatic tissues. Hybridization and post hybridization washes were conducted according to standard procedures (Alamri et al., 2017). Slides were visualized on an Olympus BX61 microscope.

18S rRNA sequencing and mycobiome analysis

For 18s rRNA sequencing fresh stool and tumor tissues were used. Approximately 25 mg of tissue samples were first homogenized with using Navy RINO Lysis Kit in a Bullet Blender Homogenizer (Next Advance) for 5 min followed by overnight treatment with proteinase K (2.5 μg/mL; Thermo Fisher Scientific, Cat.: EO0491) at 55°C. Subsequently, DNA extraction was performed using Qiagen DNeasy Powersoil Pro Kit as per manufacturer's instructions (Qiagen, Cat.: 47014). Quantitative assessment of the purified DNA was then accomplished by using a Qubit Broad Range DNA kit (Thermo Fisher Scientific, Cat.: Q32853). The sequencing libraries were prepared using a two-step PCR method using the primer set ITS1F (5′-CTTGGTCATTTAGAGGAAGTAA-3′) and ITS2 (5′-GCTGCGTTCTTCATCGATGC-3′) (Table S1). The first PCR (25-cycle) uses 25 ng of DNA to amplify the target region, where the PCR primers have overhang adapter sequence necessary for the second PCR step. After purification, the amplicon from the first step is amplified with 8 cycles of PCR using the Nextera Index Kit (Illumina Inc.), which uses primers that target the overhang adaptor sequence added during the first round of PCR. The second round PCR adds one of 384 different combinations of indexed tags to each sample which allows pooling of libraries and multiplex sequencing. Prior to pooling, each individual sample's amplified DNA is visualized on a Tapestation 4200 D1000 tape (Agilent Technologies) for expected amplicon size, purity and concentration. Validated libraries are pooled equal molar in a final concentration of 4 nM in Tris-HCl 10 mM, pH 8.5, before 2 × 300 cycle sequencing on a MiSeq (Illumina, Inc.).

Mycobiome analysis

Paired-end fastq reads were demultiplexed, processed and analyzed using QIIME (v1.9.1) (Caporaso et al., 2010). Then, operational taxonomic units (OTUs) were assigned using QIIME's uclust-based open-reference OTU-picking pipeline. OTUs with less than 0.001% assigned sequences were removed from each sample to avoid biased and inflated diversity estimates. ITS samples were processed following the QIIME pipeline steps using UNITE's Fungi taxon (v8.4) (Koljalg et al., 2013) reference-annotation adapted for QIIME. Chimeras were removed before taxonomy assignments with vsearch (v2.15.0) (Rognes et al., 2016) using the UCHIME reference dataset (v7.2) available at the UNITE website (Abarenkov et al., 2010). Positive and negative control samples were checked for QC purposes.

Taxonomy assignments from all samples were then compiled in a raw-counts matrix. Raw counts were formatted, processed, and analyzed using phyloseq package (v1.28.0) (McMurdie and Holmes, 2013) [8] in R (v4.0.0). 16S data is summarized to OTUs at the genus level. Observed, Chao1, Shannon and Simpson's Reciprocal diversity indices were estimated for alpha-diversity scores; mean estimates were obtained performing 100 bootstrapped rarefactions. Same analyses were performed for ITS, but at the species and genus levels. For Beta-diversity, Bray-Curtis dissimilarity score paired with classical multidimensional scaling was estimated and plotted using the vegan package (v2.5.6) (Oksanen et al., 2007).

Enzyme linked immunosorbent assay (ELISA)

ELISA was done using cell culture conditioned media from PDAC mouse cell lines and ascites fluid from PDAC tumor bearing mice. Cell culture media was concentrated using Amicon Ultra centrifugal filter units (Millipore, Z717185) before conducting ELISA. IL-33 ELISA was performed using LEGEND MAX Mouse IL-33 ELISA Kit (Biolegend) using manufacturer's standard protocol. IL-5 ELISA was performed using Mouse IL-5 Quantikine ELISA Kit (R&D systems) using manufacturer's standard protocol.

Please cite this article in press as: Alam et al., Fungal mycobiome drives IL-33 secretion and type 2 immunity in pancreatic cancer, Cancer Cell (2022), https://doi.org/10.1016/j.ccell.2022.01.003

ILC2 enrichment and adoptive transfer of ILC2

Orthotopically transplanted PDAC tumors (donor) were minced, and single cell suspension was prepared using mouse tumor dissociation Kit (Milteny biotec). Ficoll column was used to separate the immune cells. ILC2 cells was purified using ILC2 enrichment kit (Stem cells Technology, Cat.: 19842) according to manufacturer's instructions. Orthotopically transplanted PDAC tumor bearing mice (recipient) were used for adoptive transfer experiments. After 10 days of orthotopic pancreatic injections of PDAC cells, 1×10^5 ILC2 cells were adoptively transferred via retroorbital injection. Tumor progression was monitored using MRI imaging post transplantation and volume was measured. Mice were sacrificed between day 28–30 and tumor weight was measured. For localization of adoptively transferred ILC2 cells in the orthotopically transplanted mouse tumor, injected ILC2 cells was labeled with a lipid binding dye DiD′ solid (1,1′-Dioctadecyl-3,3,3′,3′-Tetramethylindodicarbocyanine, 4-Chlorobenzene sulfonate Salt (Invitrogen, D7757). After 7 days, PDAC tumor is harvested and DiD-labelled ILC2 cells were measured by flow cytometry using APC channel.

ILC2 Co-transplantation

For co-transplantation experiment, PDAC cells (5×10^5) were co-transplanted with ILC2 cells (2×10^5). The ILC2 cells used for this experiment was isolated as described in ILC2 adaptive transfer experiment described above. PDAC cells and ILC2 cells were mixed with Matrigel (Corning, USA) in 1:1 ratio and orthotopically injected into mouse pancreas. Tumor progression was monitored using MRI imaging post transplantation and tumor size and volume was measured. Mice were sacrificed between day 28–30 and tumor weight was measured.

QUANTIFICATION AND STATISTICAL ANALYSIS

Statistical analysis

GraphPad Prism software was used to conduct the statistical analysis of all data except for qRT-PCR data, where Microsoft excel was used. Data are presented as mean ± SD. All quantitative results were assessed by unpaired Student's *t*-test after confirming that the data met appropriate assumptions (normality and independent sampling). The Student *t*-test assumed two-tailed distributions to calculate statistical significance between groups. Unless otherwise indicated, for all *in vitro* experiments, three technical replicates were analyzed. Sample size estimation was done taking into consideration previous experience with animal strains, assay sensitivity and tissue collection methodology used. Animal survival impact was determined by the Kaplan-Meier analysis. $p < 0.05$ was considered statistically significant; the p values are indicated in the figures.